GSA Data Repository 2015313

Is the vertebrate-defined Permian–Triassic Boundary in the Karoo Basin, South Africa, the terrestrial expression of the End Permian marine event?

Gastaldo, Kamo, Neveling, Geissman, Bamford, and Looy

DR1: Vertebrate Paleontology

We have collected new vertebrate fossils from Old Lootsberg Pass sections. A partial dicynodontoid skull, the assignment of which is supported by the presence of a labial fossa behind the canine (The Albany Museum specimen AM.3659; Fig. DR1), has been recovered from the basal PNC lithofacies (S31° 47.773, E024° 47.781 ± 4m, WGS80 datum; Figs. 1, 2). The specimen displays particularly large-diameter canines, the basal diameter of which is 35 mm, decreasing to 25 mm at a point where the tusk begins to taper. These features are indicative of latest Permian taxa and, although its preservational state precludes assignment to a specific taxon, possible systematic affinities include *Dicynodon*, *Daptocephalus* and *Lystrosaurus mccaigi* (B. deKlerk, C. Kammerer, pers. comm. 9/2013).

DR2: Blaauwater Palynology

The palynological assemblage of the Blaauwater Farm is consistent with macrofloral observations of a low-diversity glossopterid woodland with an understory of sphenophytes, but also indicates the presence of a variety of other gymnosperms, peltasperms, corystosperms and conifers that are not represented in the time-equivalent macrofossil records. Spores of Sphenophyllales (*Columnisporites ovalis*, *Laevigatosporites* sp.) are dominant (~85%). Both taxa likely represent *Trizygia speciosa* (Prevec et al., 2012). *Columinisporites*, monolete spores with a ridged perispore, are known in situ from several Paleozoic sphenopsid cone taxa (e.g., Potonie, 1962; Riggs and Rothwell, 1985; Taylor, 1986). If the perispore was not preserved, the spores fall within the dispersed spore genus *Laevigatosporites* (Balme, 1995; Playford and Dino, 2000). In Gondwana, several morphospecies of multi-taeniate dispersed pollen genera are mainly associated with glossopterids (Balme, 1995; Lindström et al., 1997). Species of *Protohaploxypinus* and *Striatopodocarpites* have been found in situ in pollen sacs that are morphologically identical to those found in attachment to glossopterid pollen organs (Surange and Chandra, 1975; Zavada, 1991; Pant and Nautiyal, 1960; Lindström et al., 1997). *Weylandites* is known from a pollen organ with a potential glossopterid affinity (Pant and Basu, 1977; Balme, 1995). In this assemblage, these pollen taxa of glossopterid affinity (*P. limpidus*, *S. cancellatus*, and *W. lucifer*) were relatively common (1-5%). Taeniate bisaccate *Lueckisporites virkkiae*, *Guttulapollenites hannonicus*, and *Lunatisporites noviaulensis* pollen (all common), were likely produced by peltasperm seedferns and conifers (e.g., Clement-Westerhof, 1987), groups that are not represented in the macrofloras. The bisaccate alete pollen genera *Falcisporites* and *Alisporites*, are known to represent corystosperm and peltasperm seedferns (Zavada and Crepet, 1985; Balme, 1995; Lindström et al., 1997). *Falcisporites australis* (common) is reported from the Early Triassic peltasperm *Lepidopteris* (Retallack, 2002; Lindström et al., 1997). *Alisporites* was produced by *Autunia*, an Euramerican Permian peltasperm, and voltzian conifers (Balme, 1995). To which group the producer *A. tenuicorpus* (common) belonged is unknown. To date, there is no conclusive macrofossil evidence for peltasperms, corystosperms, or conifers from Late Permian Karoo Basin macrofloras. Pollen types associated with these groups could either represent para-autochtonous or allochthonous elements or plant groups known from the basin but with which they have hitherto not been associated.

DR3: U-Pb ID-TIMS Geochronology Methodology

Zircon grains were pretreated by chemical abrasion to remove radiation-damaged and altered zones (Mattison, 2005) by placing them in a muffle furnace at ~1000° C for ~48 hours to anneal radiation damage, followed by partial dissolution in 50% HF in Teflon dissolution vessels at 200° C for approximately 17 hours. Each zircon fragment was cleaned in HNO_3, and transferred to a miniaturized Teflon bomb (Krogh et al., 1973). A mixed ^{205}Pb-$^{233-235}$U spike was added to the Teflon dissolution capsules during sample loading (EARTHTIME community tracer, to facilitate inter-laboratory comparisons, see www.earth-time.org). Zircon was dissolved using ~0.10 ml concentrated HF acid and ~0.02 ml 7N HNO_3 at 200° C for 5 days, and re-dissolved in ~0.15 ml of 3N HCl. Uranium and lead were isolated from the zircon solutions using anion exchange columns, dried down with dilute phosphoric acid, deposited onto out gassed rhenium filaments with silica gel (Gerstenberger and Haase, 1997), and analyzed with a VG354 mass spectrometer using a Daly detector in pulse counting mode. Corrections to the ^{206}Pb-^{238}U and ^{207}Pb/^{206}Pb ages for initial ^{230}Th disequilibrium in the zircon data have been made assuming a Th/U ratio in the magma of 4.2. Laboratory procedural blanks are routinely at the 0.5 pg and 0.1 pg level for Pb and U, respectively. All common Pb was assigned to procedural Pb blank. Dead time of the counting system for Pb was 16 ns and 14 ns for U. The mass discrimination correction for the Daly detector is constant at 0.05% per atomic mass unit. Amplifier gains and Daly characteristics were monitored using the SRM 982 Pb standard. Thermal mass discrimination correction for Pb is 0.10 % per atomic mass unit. U fractionation was measured internally and corrected for each cycle. Decay constants are those of Jaffey et al. (1971), and age calculations were done using an in-house program by D.W. Davis. All age errors quoted in the text and table, and error ellipses in the Concordia diagrams are given at the 95% confidence interval. Plotting and age calculations were done using Isoplot 3.00 (Ludwig, 2003). Data presented in Table DR1.

The porcellanite contains abundant unaltered, euhedral, elongate, equant and multi-faceted zircon grains. U-Pb analysis of 11 single grains produced data for four that are interpreted as antecrysts, or inherited due to post depositional recycling in the sedimentary environment or inclusion during magmatic ascent/emplacement. Data for the remaining seven grains have overlapping $^{206}Pb/^{238}U$ ages that together have a weighted mean of 253.48 ± 0.15 Ma (2 σ; MSWD=0.47), which is interpreted as the best age estimate of the main zircon population and a maximum for the time of porcellanite deposition (Fig. DR2). This age places the porcellanite in the early Changhsingian (254.2-251.9 Ma).

DR4: Magnetic Polarity Stratigraphy, Old Lootsberg Pass Section

Methods

Where possible, samples for magnetic polarity stratigraphy were collected by drilling oriented cores using a portable field drill with a non-magnetic diamond drill bit. Typically, seven to 12+ independently-oriented drill samples were obtained from each suitable bed in the Old Lootsberg Pass section discussed in this paper (Table DR2). Most beds sampled are exposed in the main donga where the section was measured and described (Fig. 1). Most beds sampled are medium to coarse grained siltstones and very fine sandstones. Several nodular (concretions) horizons in fine siltstones/mudstones also were sampled. The number of independently oriented samples obtained is relatively high for magnetic polarity stratigraphy investigations. This is because of the implicit need to fully characterize the magnetization in the rocks of this section and to convincingly assess the homogeneity, or lack thereof, of the remanence at each stratigraphic level, as opposed to all previous studies of presumably uppermost Permian and lowermost Triassic strata in this part of the Karoo Basin. In part, this is due to the extensive suite of mafic (diabase) intrusions of the Early Jurassic Karoo Large Igneous Province that were emplaced throughout the eastern Cape. In the eastern Cape, most of these intrusions are of normal polarity

(Geissman and Ferre, 2013) and, therefore, separating an inferred early acquired, normal polarity remanence in uppermost Permian and lowermost Triassic strata from a normal polarity Early Jurassic "overprint" is not necessarily straightforward, as noted in selected parts of the Karoo Basin (Lanci et al., 2013; Mare et al., 2014). Published paleomagnetic results from strata encompassing the Permo-Triassic boundary sequence in the central Karoo Basin (eastern Cape) are exceptionally poorly documented and confusing. There is absolutely no evidence, for example, based on the data reported, that reverse polarity magnetozones that are defined by well-behaved, stable endpoint magnetizations, exist in any of the sections reported by Ward et al. (2005).

Core samples were processed into standard 2.2 cm high specimens for remanence and rock magnetic measurements. Each specimen, after processing, was washed in dilute HCl to remove any form of metal contamination after specimen preparation. For those stratigraphic intervals lacking beds suitable for drilling, samples were collected as oriented blocks of a range of sizes by marking the orientation of any flat surface of a block that could be removed from the outcrop. Typically five to eight oriented blocks were obtained from a single (< 0.5 m) stratigraphic interval. The oriented block samples were recut into multiple 2.0 cm cubical specimens using a non-magnetic diamond saw blade. We NOTE THAT the nomenclature for our magnetostratigraphic sample collection utilizes a "WLP" prefix (West Lootsberg Pass, synonymous with Old Lootsberg Pass).

Remanence measurements were made on either a 2G Enterprise, DC SQUID, three-axis pulse cooled superconducting rock magnetometer, interfaced with an automated specimen handler and an on-line alternating field (AF) degausser system, or JR5A or JR6A AGICO spinner magnetometers inside a large (Texas-sized) magnetic shield (Version #50 of Lodestar Magnetics) with an ambient field of less than 300 nT in most areas.

Because the principal magnetic phase in strata of the Old Lootsberg Pass section strata is mainly magnetite, although hematite carries part of the remanence at some sites, as shown below, specimens from samples from all sites were subjected to both thermal and alternating field (AF) demagnetization. Thermal demagnetization was carried out using one of three ASC TD48, dual zone thermal demagnetizer, in a progressive fashion involving 20 to 30 steps to maximum laboratory unblocking temperatures of 680°C (+/-). AF demagnetization was carried out using the integrated 2G Enterprises AF demagnetization system, typically to peak fields of 90 to 120 mT.

Acquisition of isothermal remanent magnetization (IRM) and backfield demagnetization of saturation IRM utilized an ASC multi-coil impulse magnet system. Three component thermal demagnetization of IRM acquired in different DC fields followed the method of Lowrie (1990). Anisotropy of magnetic susceptibility (AMS) determinations were made using either KLY-3S or a MFK1A AGICO automated magnetic susceptibility instruments. Measurements of the variation in magnetic susceptibility as a function of heating and cooling were carried out on magnetic separates from powders of block samples collected from selected sites using an AGICO CS-4 apparatus interfaced with a MFK1A susceptibility instrument. These measurements were conducted in an argon atmosphere. All remanence measurements and demagnetization procedures were performed in a magnetic shield constructed by Lodestar Magnetics.

Results of progressive demagnetization were inspected using orthogonal demagnetization diagrams (Zijderveld, 1967) and the directions of magnetization components identified by the colinearity of several demagnetization data points determined using principal components analysis (Kirschvink, 1980). Magnetization directions at the site level were estimated as mean directions using as many independent observations as accepted, following the method of Fischer (1953). These estimated site mean magnetization directions were transformed into virtual geomagnetic poles (VGPs) and plotted on the cumulative stratigraphic column (Opdyke and Channel, 1966) to reveal the magnetic polarity stratigraphy of our section. Estimated paleomagnetic pole positions (Van der Voo, 1993; Torsvik et al., 2012; Muttoni et al., 2013) for Africa for Late Permian/Early Triassic time are such that normal polarity magnetizations in these strata in the Groot Karoo in the eastern Cape of South Africa should have a north-northwest declination and moderate to steep negative (at least - 60°) inclination magnetization.

Paleomagnetic and Rock Magnetic Results

Intensities of the natural remanent magnetization in the rocks sampled in the Old Lootsberg Pass section range from about 5 mA/m to 0.1 mA/m. Specimens from most samples from all sites studied to date from the Old Lootsberg Pass section yield a first-removed, well-defined northwest to north-northwest moderate to steep negative inclination magnetization, thus of normal polarity (Figs. DR3, DR4). This magnetization component is comparable to the present day field direction for the eastern Cape of about 334.7° and -64.8° (WMM 2010). It is also, notably as above, comparable to the direction of the characteristic remanent magnetization of mafic intrusive igneous rocks of the Early Jurassic (ca. 184 Ma) Karoo Large Igneous Province (Hargraves et al., 1997; Geissman and Ferre, 2013), which are predominantly of normal polarity in this area of southern Africa. In most, but not all, sites, this is the principal magnetization component isolated and is unblocked over a range of laboratory unblocking temperatures to about 580° C and randomized in AF demagnetization by 80 to 100 mT. At the site (=bed) level, the within site (between-sample) consistency in magnetization character is very high. The typical maximum laboratory unblocking temperatures of ~580° C and median destructive fields of 20 to 40 mT are interpreted to suggest that magnetite is the principal carrier of the remanence in these rocks. IRM acquisition and backfield demagnetization curves (Fig. DR5) support this interpretation. Specimens reach full or nearly full saturation by about 200 mT, and yield coercivities of remanence of about 40-50 mT. The geometric form of the IRM acquisition curves and the values of coercivity of remanence are consistent with contributions by magnetite grains in the pseudo-single domain size range. A comparison of the response to progressive alternating field demagnetization of the NRM, ARM (peak AF field of 100 mT), and IRM (peak DC field of 100 mT; Fig. DR6) indicates that fine, pseudo-single domain magnetite is an important component of the magnetic mineralogy in these rocks. Transmitted and reflected light examination of polished thin sections of samples from selected sites reveals the presence of rare, fine (<< 50 micron diameter), subrounded to rounded magnetite grains as part of the detritus (Fig. DR7). In reflected light, the magnetite grains appear unoxidized. The lack of abundant, obvious detrital magnetite grains with sizes comparable to the typical relatively coarse silicate detritus is consistent with the relatively low NRM intensities of these rocks and their rock magnetic behavior.

Magnetic separates from hand samples from selected sites required careful preparation from a large volume of crushed material. The best separates that we could obtain (e.g., site WLP 13) all show a substantial decrease in susceptibility at about 580° C (Fig. DR8), indicative of nearly pure magnetite as the principal magnetic phase. The heating curves show a slight Hopkinson effect, demonstrating the presence of at least some multidomain magnetite. The initial heating/cooling curves are close to reversible. A second heating/cooling cycle shows the reversibility of the curves.

Anisotropy of magnetic susceptibility (AMS) from these rocks are consistent with the preservation of a primary depositional fabric (Fig. DR9) with Kmin axes oriented close to vertical, and Kmax and Kint axes either relatively well grouped with sub-horizontal orientations or they are distributed in a sub-horizontal plane. At the site level, the degree of anisotropy (P) ranges from 1.002 to 1.050, with most sites having P values between about 1.020 and 1.030.

Discussion of Results

In terms of a magnetic polarity stratigraphy for the Old Lootsberg Pass section studied, to date, with the exception of one narrow stratigraphic interval centered around site WLP17 (and correlative to adjacent sites WLP 103/WLP 104), all sites examined in sufficient detail to date show the presence of a normal polarity magnetization as the principal and only well-defined component of the NRM. All samples from site WLP17, on the other hand (highlighted in Fig. DR4, Part 2), show the unblocking of a normal polarity magnetization and then the consistent isolation of a remanence of south-southeast declination and moderate positive inclination (thus of reverse polarity). In a few additional sites, to date, there is a consistent hint of the presence of a magnetization that is south-directed and of moderate positive inclination, but this magnetization, if it is real, is often a small percentage of the NRM and is often not well-defined. Is the normal polarity magnetization that is the principal component of the NRM in these rocks simply a complete, or nearly complete overprint or "remagnetization" associated with Karoo magmatism? Based on our ongoing magnetic polarity stratigraphic work on other upper Permian/lower Triassic sections in the eastern Cape, the most likely answer is that it is not. In some cases, the normal polarity magnetization is clearly unblocked by laboratory unblocking temperatures of about 450º C, and a magnetization that is south-directed and of moderate positive inclination (interpreted as reverse polarity) is isolated at higher temperatures (Geissman, work in progress). Consistent with the observations of Lanci et al. (2013), normal polarity magnetizations that are isolated at temperatures above about 450º C are interpreted as early-acquired, likely primary magnetizations. Overall, our interpretation is also consistent with the magnetic geothermometry work reported by Mare et al. (2014), who, based on experiments on continuous drill core obtained at several localities in the Karoo Basin, concluded that sedimentary strata of the Karoo Supergoup experienced maximum temperatures between about 200° C and about 650° C, presumably prior to and during the time of Karoo Large Igneous Province magmatism. The highest maximum temperatures were derived from rocks within the thermal aureole of Karoo sills. For sedimentary strata spatially removed from and between sills, Mare et al. (2014) reported lower limits of estimated maximum temperature values between 200 and 300° C. They also emphasized that their work implies that Karoo sill intrusion "did not completely overprint the magnetic signatures of Karoo sedimentary strata". We thus conclude, given the available data and our present sampling coverage, that the sedimentary strata of the Old Lootsberg Pass section we report on in this paper do contain early-acquired magnetizations and that these strata lie largely within a magnetozone of normal polarity or, thus, a time interval dominated by normal polarity chrons.

ADDITIONAL REFERENCES

BALME, B.E., 1995, Fossil *in situ* spores and pollen grains: an annotated catalogue: Review of Paleobotany and Palynology, v. 87, p. 81-323.

CLEMENT-WESTERHOF, J.A., 1987, Aspects of Permian palaeobotany and palynology, VII. The Majonicaceae, a new family of Late Permian conifers. Review of Paleobotany and Palynology, v. 52, p. 375-402.

FISHER, R.A., 1953, Dispersion on a sphere: Proceedings of the Royal Society of London, v. A217, p. 295-305.

GEISSMAN, J.W., AND FERRE, E.C., 2013, Paleomagnetism of Early Jurassic igneous rocks of the Karoo Large Igneous Province, South Africa, and an evaluation of Karoo paleomagnetic data bearing on the recently postulated Jurassic true polar wander event: Geological Society of America Abstracts with Programs, v. 45, p. 811.

GERSTENBERGER, H., AND HAASE, G., 1997, A highly effective emitter substance for mass spectrometric Pb isotope ration determinations: Chemical Geology, v. 136, p. 309–312.

HARGRAVES, R.B., REHACEK, J., AND HOOPER, P.R., 1997, Palaeomagnetism of the Karoo igneous rocks in southern Africa: South African Journal of Geology, v. 100, p. 195-212.

JAFFEY, A.H., FLYNN, K.F., GLENDENIN, L.E., BENTLEY, W.C., AND ESSLING, A.M., 1971, Precision measurement of half-lives and specific activities of ^{235}U and ^{238}U: Physical Review C, v. 4, p. 1889-1906.

KIRSCHVINK, J.L.., 1980, The least squares line and plane and the analysis of paleomagnetic data: Geophysical Journal of the Royal Astronomical Society, v. 62, p. 699-718.

KROGH, T.E., 1973, A low contamination method for hydrothermal decomposition of zircon and extraction of U and Pb for isotopic age determinations: Geochimica Cosmochimica Acta, v. 37, p. 485-494

LANCI, L., TOHVER, E., WILSON, A., AND FLINT, S., 2013, Upper Permian magnetic stratigraphy of the lower Beaufort group, Karoo basin: Earth and Planetary Science Letters, v. 175, v. 123-134.

LINDSTRÖM, S., MCLOUGHLIN, S., AND DRINNAN, A., 2007, Intraspecific variation of taeniate bisaccate pollen within Permian glossopterid sporangia, from the Prince Charles Mountains, Antarctica: International Journal of Plant Sciences, v. 158, p. 673-684.

LOWRIE, W., 1990, Identification of ferromagnetic minerals in a rock by coercivity and unblocking temperature properties: Geophysical Research Letters, v. 17, p. 159-162.

MARE, L.P., DE KOCK, M.O., CAIRNCROSS, B., AND MOURI, H., 2014, Application of magnetic geothermometers in sedimentary basins: An example from the western Karoo Basin, South Africa: South African Journal of Geology, v. 117, p. 1-14.

MUTTONI, G., DALLANAVE, E., AND CHANNELL, J.E.T., 2013, The drift history of Adria and Africa from 280 Ma to Present, Jurassic true polar wander, and zonal climate control on Tethyan sedimentary facies: Palaeogeography, Palaeoecology, Palaeoclimatology, v. 386, p. 415-435.

OPDYKE, N.D., AND CHANNEL, J.E.T., 1966, *Magnetic Stratigraphy*: Academic Press, San Diego, 346 pp.

Van der Voo, R., 1993, *Paleomagnetism of the Atlantic, Tethys, and Iapetus Oceans*: Cambridge University Press, Cambridge, UK, 411 pp.

Pant, D.D., and Basu, N., 1977, On some seeds, synangia and scales from the Triassic of Nidpur, India: Palaoentolgraphica B, v. 163, p. 162-178.

PANT, D.D., AND NAUTIYAL, D.D., 1960, Some seeds and sporangia of *Glossopteris* flora from Raniganj Coalfield, India: Palaoentolgraphica B, v. 107, p. 41-64.

PLAYFORD, G., AND DINO, R., 2000, Palynostratigraphy of the Upper Palaeozoic strata (Tapajós Group) Amazonas Basin, Brazil: Part Two: Palaeontologica B, v. 255, p. 87-145.

POTONIE, R., 1962, Regeln nach denen sich die Sekundarfalten der Sporen bilden: Palaontologisches Zeitschrift, v. 36, p. 46-54.

PREVEC, R., SCISCIO, L., LOOY, C., AND GASTALDO, R.A., 2012, Well-preserved impression/compressions of *Trizygia speciosa*, including the first cones and spores of this widespread Gondwanan sphenophyte, from the latest Permian of South Africa: International Organization of Palaeobotany Meetings, Tokyo, Japan, SS33-O05 (414).

RETALLACK, G.J., 2002, *Lepidopteris callipteroides*, the earliest Triassic seed fern in the Sydney Basin, southeastern Australia: Alcheringa, v. 26, p. 475-500.

RIGGS, S.D., AND ROTHWELL, G.W., 1985, *Sentistrobus goodii* n. gen et sp., a permineralized sphenophyllalean cone from the Upper Pennsylvanian of the Appalachian Basin: Journal of Paleontology, v. 59, p. 1194-1202.

SURANGE, K.R., AND CHANDRA, S., 1975, Morphology of the gymnospermous fructifications of Glossopteridales from India: Palaeontographical B, v. 129, p. 153-180.

TAYLOR, W.A., 1986, Ultrastructural studies of sphenophyllalean spores: Review of Paleobotany and Palynology, v. 47, p. 105-128.

TORSVIK, T.H., VAN DER VOO, R., PREEDEN, U., NIOCALLI, C.M., STEINBERGER, B., DOUBROVINE, P.V., VAN HINSBERGEN, D.J.J., DOMEIER, M., GAINA, C., TOHVER, E., MEERT, J.G., MCCAUSLAND, P.J.A., AND COCKS, L.R.M., 2012, Phanerozoic polar wander, palaeogeography and dynamics: Earth Science Reviews, v. 114, p. 325-368.

ZAVADA, M.S., 1991, The ultrastructure of pollen found in dispersed sporangia of *Arberiella* (Glossopteridaceae): Botanical Gazette, v. 152, p. 248-255.

Zavada, M.S., and Crepet, W.L., 1985, Pollen wall ultrastructure of the type material of *Pteruchus africanus*, *P. dubius*, and *P. papillatus*: Pollen and Spores, v. 27, p. 271-276.

ZIJDERVELD, J.D.A., 1967, Demagnetization of rocks: Analysis of results: *in* Collinson, D.W., Creer, K.M., and Runcorn, S.K., Eds., *Methods in Palaeomagnetism,* Elsevier, Amsterdam, p. 254, 286.

Figure Captions

Fig. DR1 – Partial dicynodontoid skull recovered at S31° 47.773, E024° 47.781 ± 4m (WGS80 datum). (A) Field image of partial skull as found exposed in the basal pedogenic nodule conglomerate. One large canine (arrow), maxilla, and some elements of the basicranium and posterior remnants can be seen in the outcrop. Scale in dm and cm. (B) Line illustration of generic dicynodontoid skull illustrating the skeletal elements recovered. (C) Prepared partial skull showing large canine (arrow) and maxilla. Scale in cm.

Fig. DR2 – Concordia diagram showing U-Pb data for chemically abraded single zircon grains from a volcaniclastic layer ~60 m below the purported PTB, Old Lootsberg Pass section, Karoo Basin, South Africa, dated at 253.48 ± 0.15 Ma (2σ) based on the seven youngest zircon grains (of eleven grains dated). Insets are: photomicrograph os representative zircon grains similar to those that were analyzed; a plot of $^{206}Pb/^{238}U$ ages (data for oldest not plotted).

Fig. DR3 – Examples of orthogonal progressive demagnetization diagrams[39] showing the end point of the magnetization vector plotted onto the horizontal (filled symbols) and vertical (open symbols) planes (NS-EW, EW-Up/Dn) for individual specimens from samples from selected sites sampled in the West Lootsberg Pass section that have been subjected to progressive **alternating field (AF)** demagnetization. Demagnetization steps, in peak alternating fields (in milliTesla, mT) are given alongside selected vertical projection data points. Also shown are normalized intensity decay plots showing response to progressive AF treatment (abscissa is peak alternating field, in milliTesla) and equal area stereographic projections of the magnetization vector measured at each step.

Fig. DR4 – Examples of othogonal progressive demagnetization diagrams[39] showing the end point of the magnetization vector plotted onto the horizontal (filled symbols) and vertical (open symbols) planes (NS-EW, EW-Up/Dn) for individual specimens from samples from selected sites sampled in the West Lootsberg Pass section that have been subjected to progressive **thermal** demagnetization. Demagnetization steps, in peak alternating fields (in degrees C) are given alongside selected vertical projection data points. Also shown are normalized intensity decay plots showing response to progressive treatment (abscissa is temperature, in degrees C) and stereographic projections of the magnetization vector measured at each step.

Fig. DR5 – Plots showing the acquisition of isothermal remanent magnetization (IRM) and backfield direct-field demagnetization for specimens from selected samples from sites in the West Lootsberg Pass section. In backfield demagnetization, the cross-over point gives the coercivity of remanence. The fact that saturation or near-saturation is reached by or well below 300 mT indicates that a cubic magnetic phase (magnetite/maghemite) is the principal magnetic phase present.

Fig. DR6 – Plots comparing the response of specimens from samples from selected sites in the West Lootsberg Pass section to progressive alternating field (AF) demagnetization of the natural remanent magnetization (NRM), anhysteretic remanent magnetization (ARM) (acquired in a peak AF field of 100 mT in a DC field of 0.1 mT; ovals), and isothermal remanent magnetization (IRM) acquired in a peak impulse DC field of 100 mT. For all sites, also shown (red symbols) are AF demagnetization responses of ARM and IRM, AFTER specimens have been subjected to progressive thermal demagnetization.

Fig. DR7 – Transmitted (plane and crossed polars) and reflected light photomicrographs showing two typical paragenetic relations for detrital magnetite grains in representative olive gray siltstone from two sites in the Old Lootsberg Pass section. Scale bar in each image is 20 microns.

Fig. DR8 – Plots showing the variation in bulk susceptibility vs. thermal cycling (C vs. temperature experiments). Magnetic separates obtained from hand samples collected from selected sites. In each of these diagrams, the red curve is the initial heating of the separate; blue curve is the initial cooling. Heating and cooling cycles are carried out with the magnetic separate flushed with argon gas. (a) Site WLP13, olive grey siltstone. Black curve with red squares is the second heating cycle; black curve with blue squares is the second cooling cycle. (b) Site WLP16, light grey siltstone.

Fig. DR9 – Examples of anisotropy of magnetic susceptibility (AMS) data from 18 selected sites in the West Lootsberg Pass section, arranged in stratigraphic order from lowermost site selected (WLP 115) to uppermost (WLP 61). For each site, the stereographic projection shows the principal susceptibility axes for each specimen measured (lower hemisphere projections). In addition, the anisotropy parameter P, where P = Kmax/Kmin, is plotted vs. bulk susceptibility for each specimen measured and the anisotropy parameter T, where T, the shape parameter (= ([2lnKint – ln Kmax – lnKmin]/[lnKmax – lnKmin]) is plotted vs. P. T values close to 1.0 are associated with strong oblate fabrics. The data from each site, with the exception of site WLP107, show a fabric that is typical of very fine grained detrital sedimentary rocks, with the minimum susceptibility axis essential vertical and well-grouped. Some sites (e.g., WLP21, WLP 24, WLP 29, and WLP61, all in coarser, fine sandstones vs. typical siltstones) display a well-defined imbrication fabric, with the minimum susceptibility axis canted from the vertical. Site WLP 107 was established in several 0.5 m + diameter concretions at a specific stratigraphic datum.

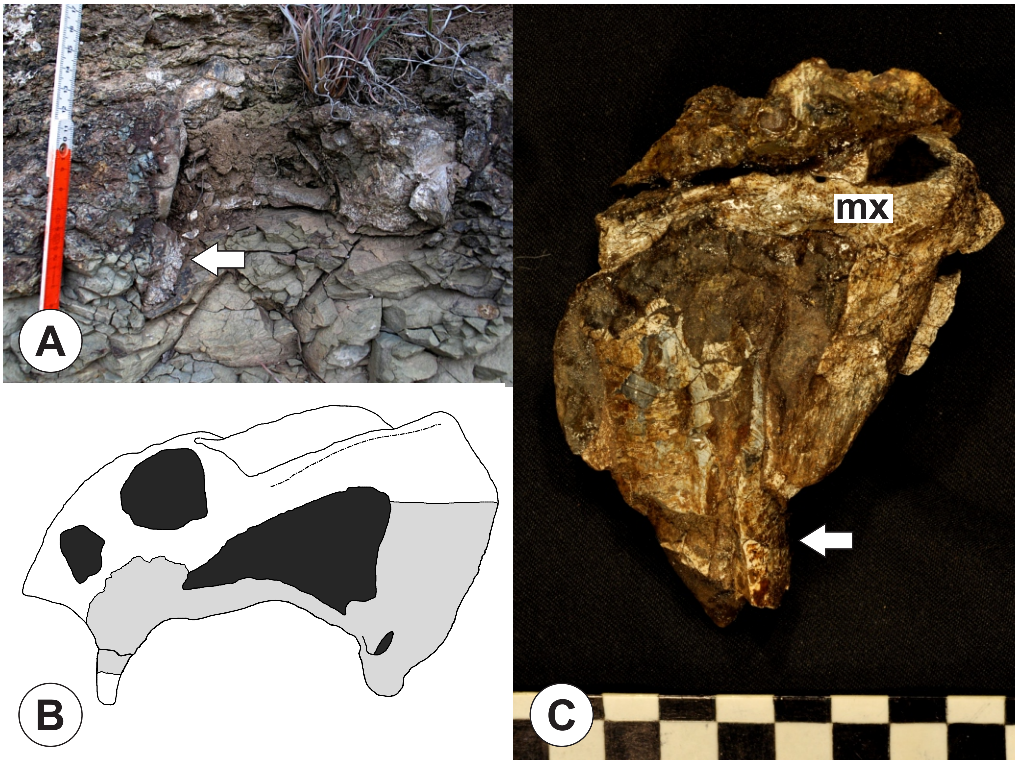

Gastaldo et al.; Fig. DR1

Old Lootsberg Pass

porcellanite layer; CA-ID-TIMS single zircon grains

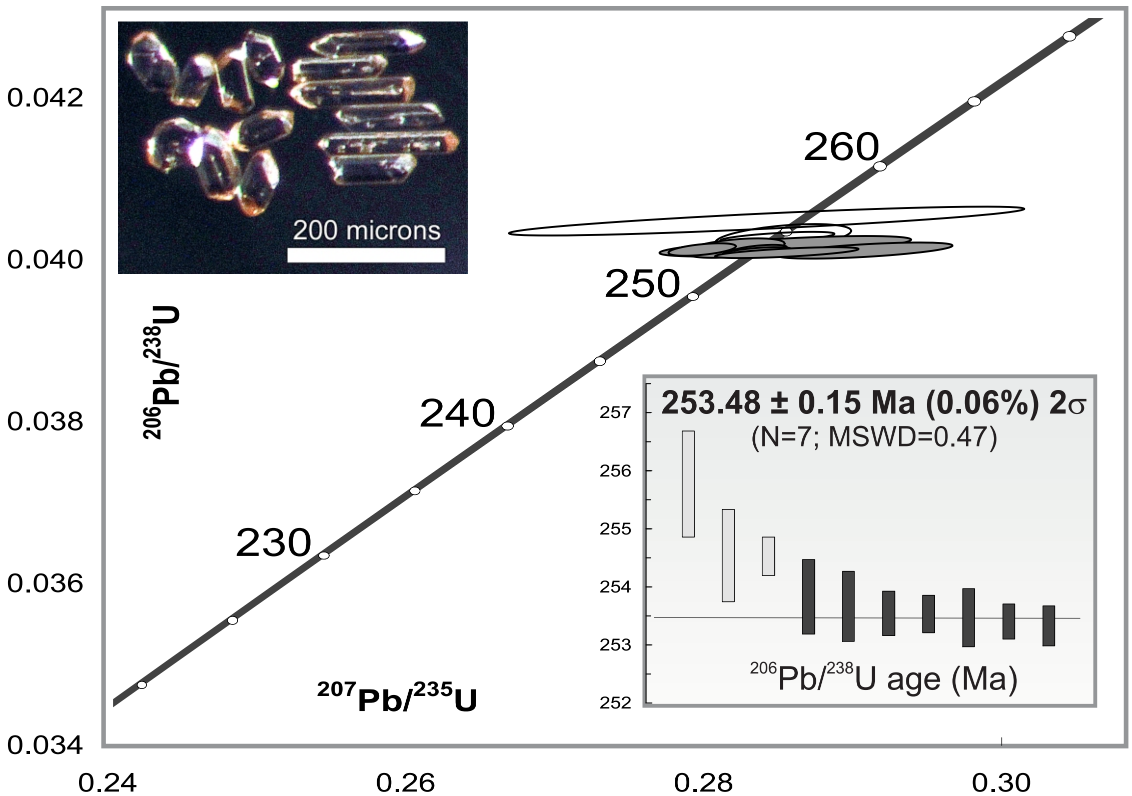

Gastaldo et al.; Fig. DR2

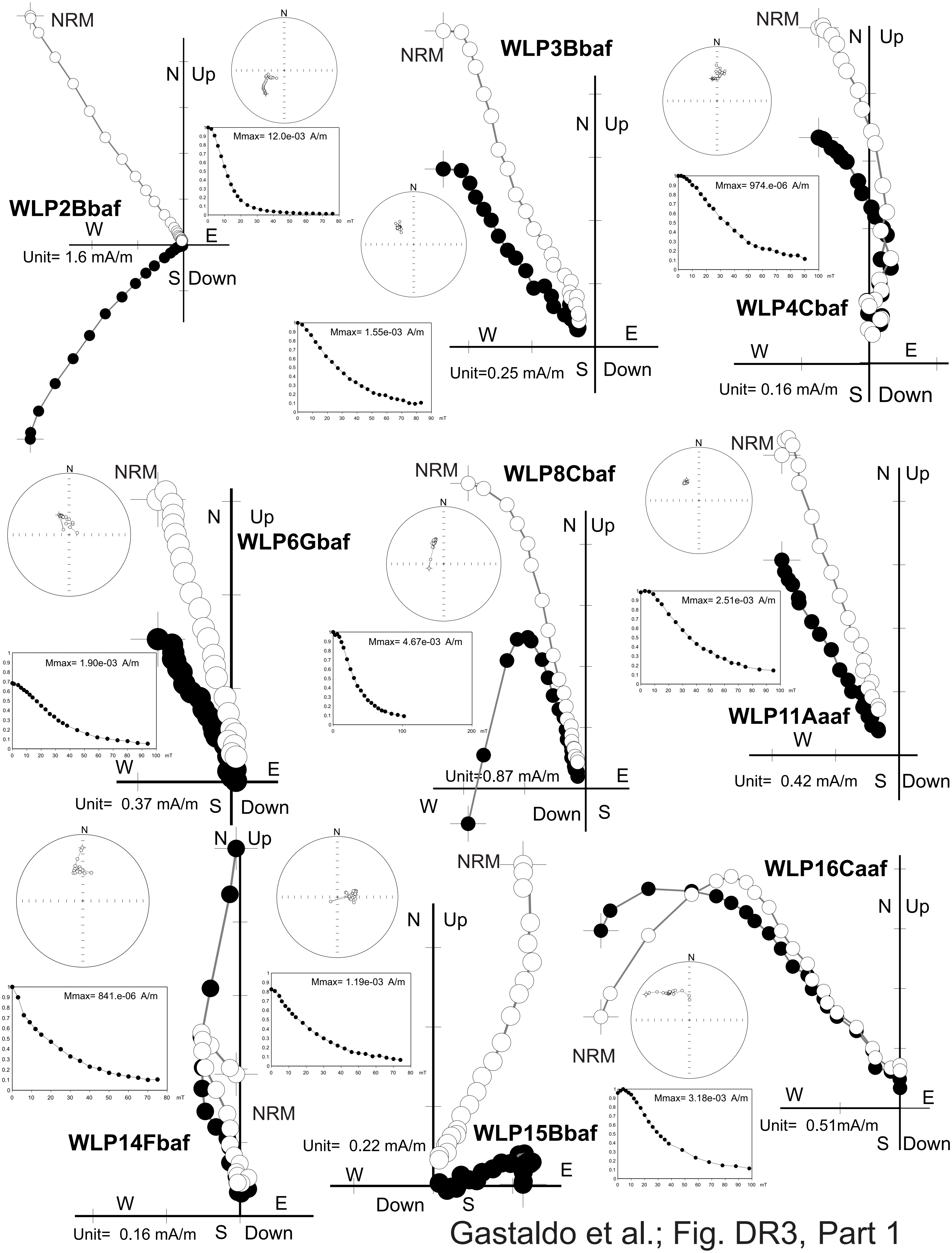

Gastaldo et al.; Fig. DR3, Part 1

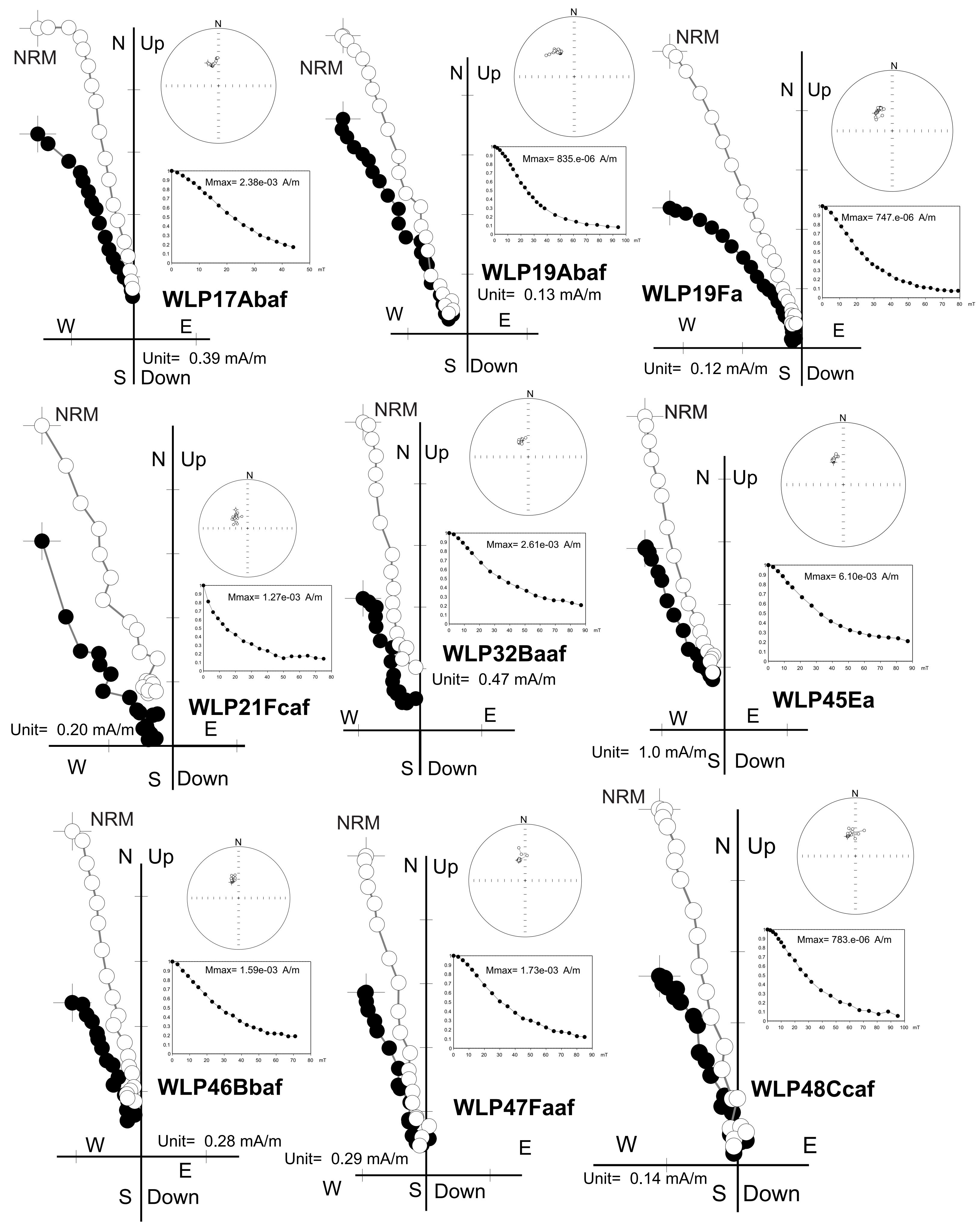

Gastaldo et al.; Fig. DR3, Part 2

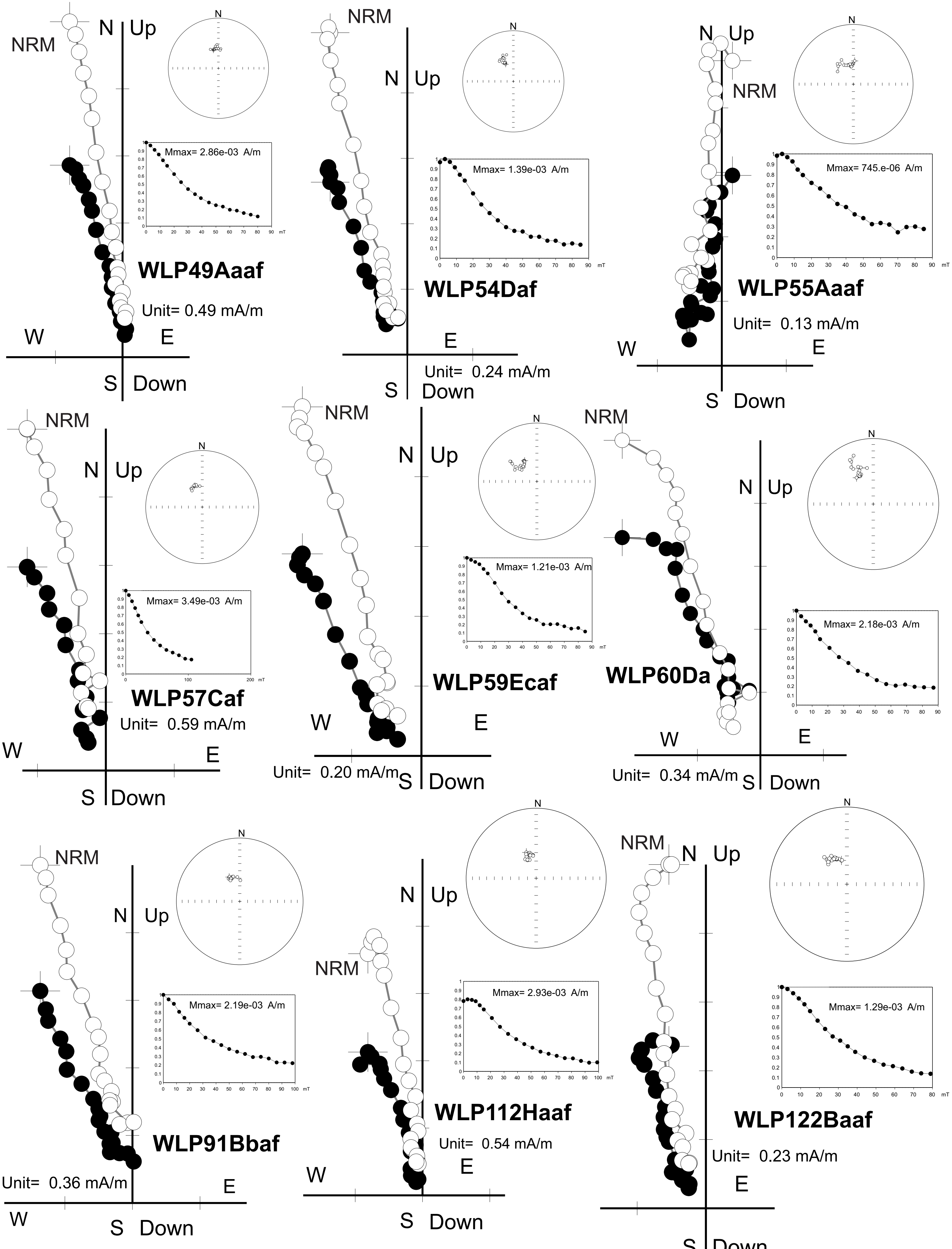

Gastaldo et al.; Fig. DR3, Part 3

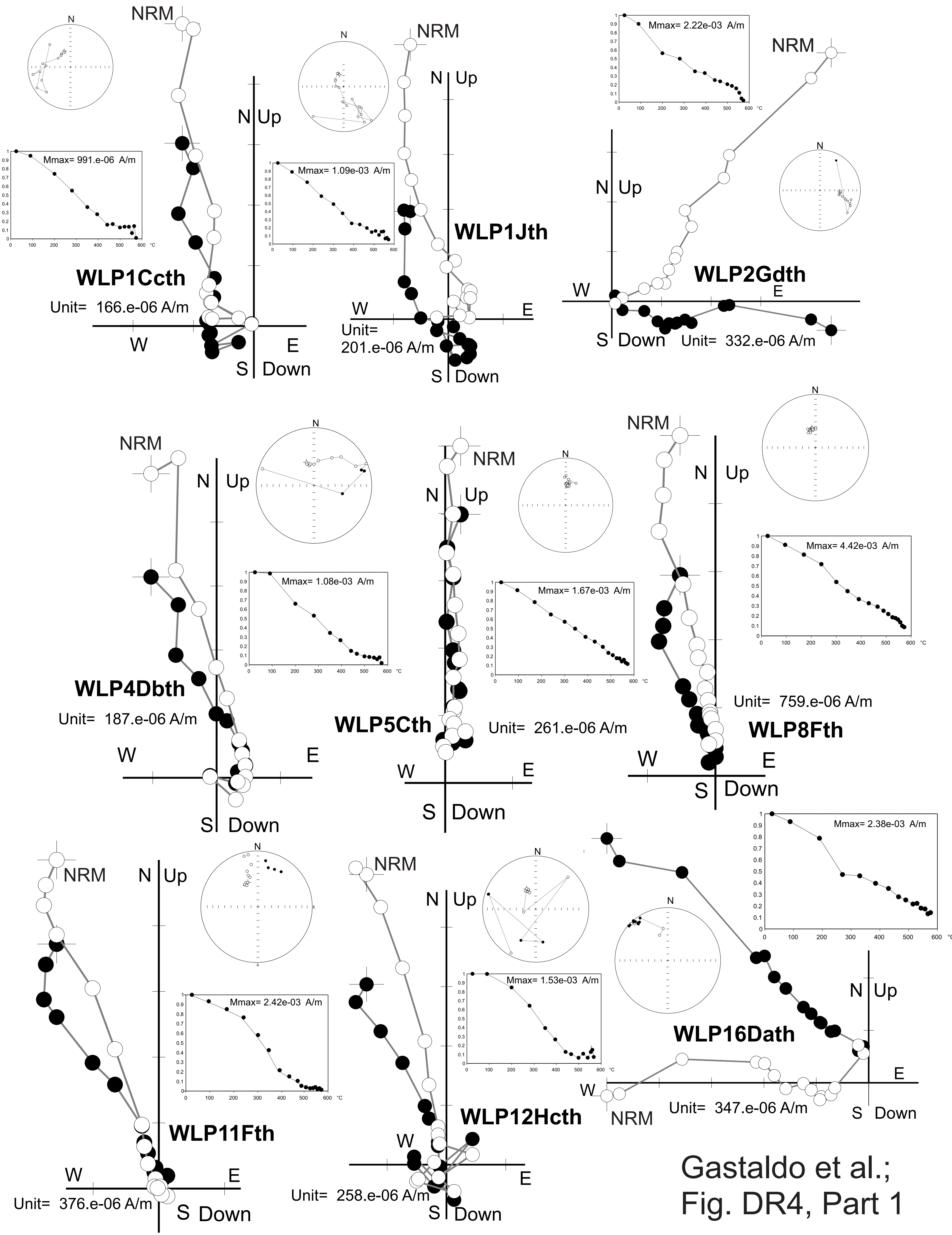

Gastaldo et al.;
Fig. DR4, Part 1

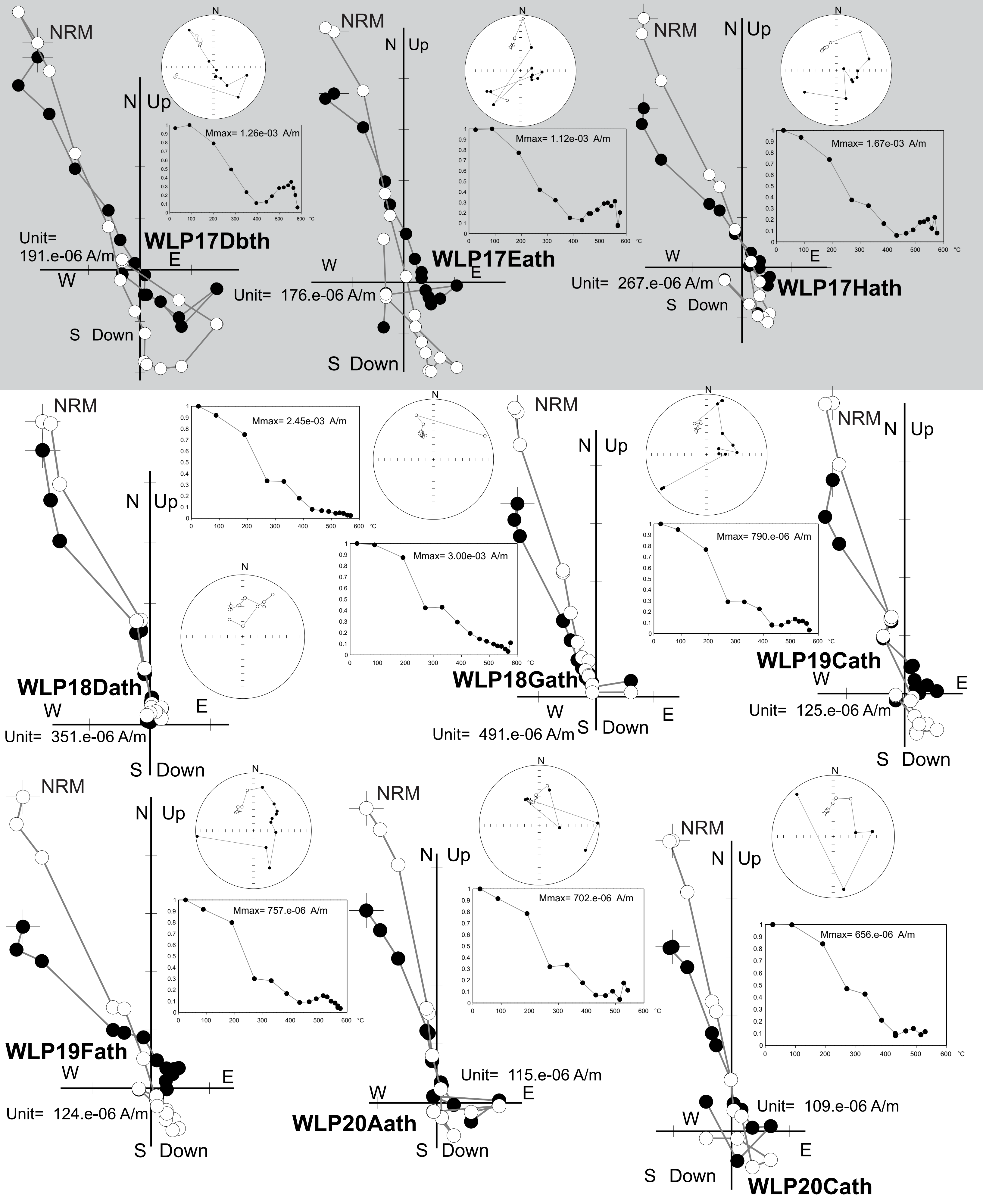

Gastaldo et al.; Fig. DR4, Part 2

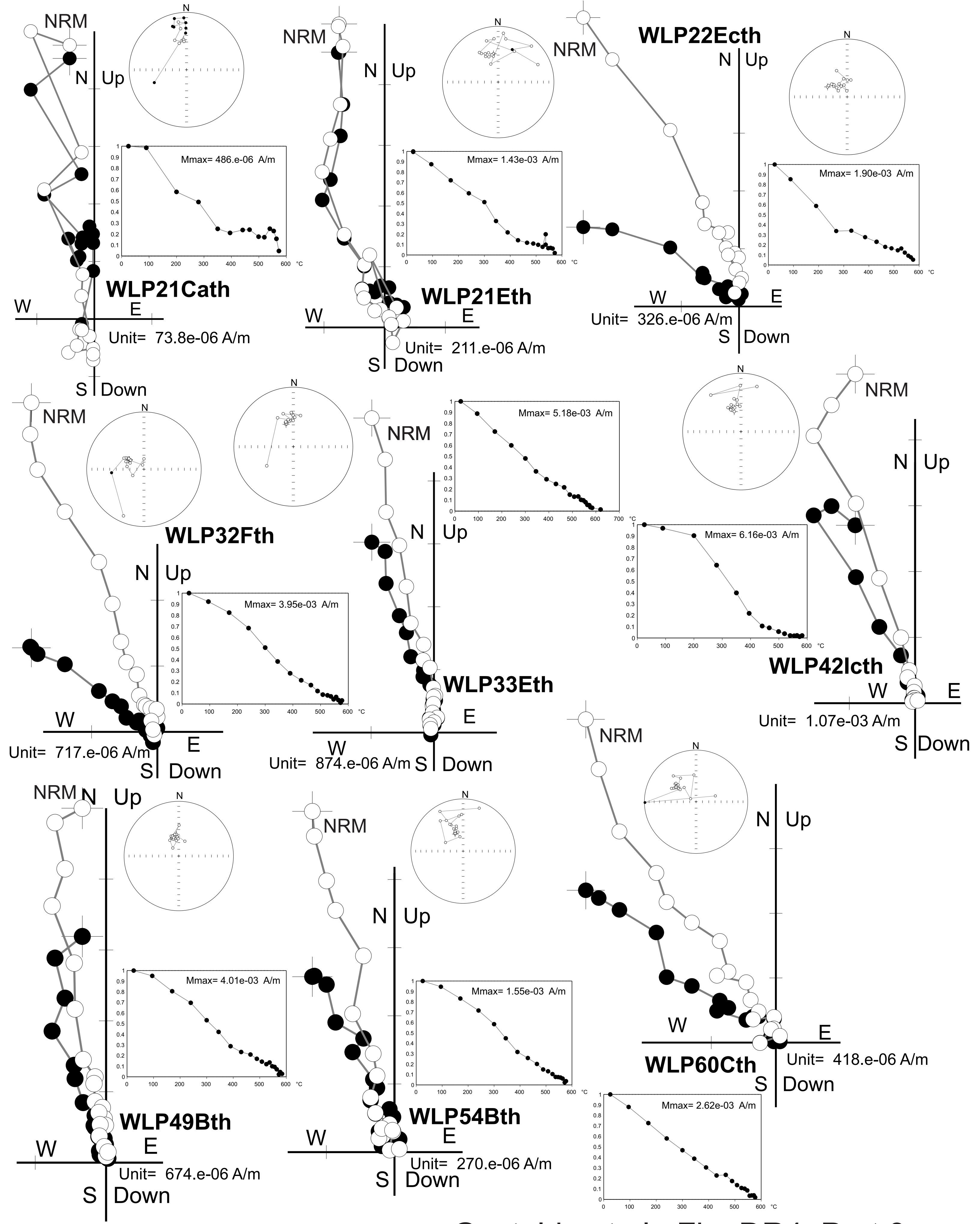

Gastaldo et al.; Fig. DR4, Part 3

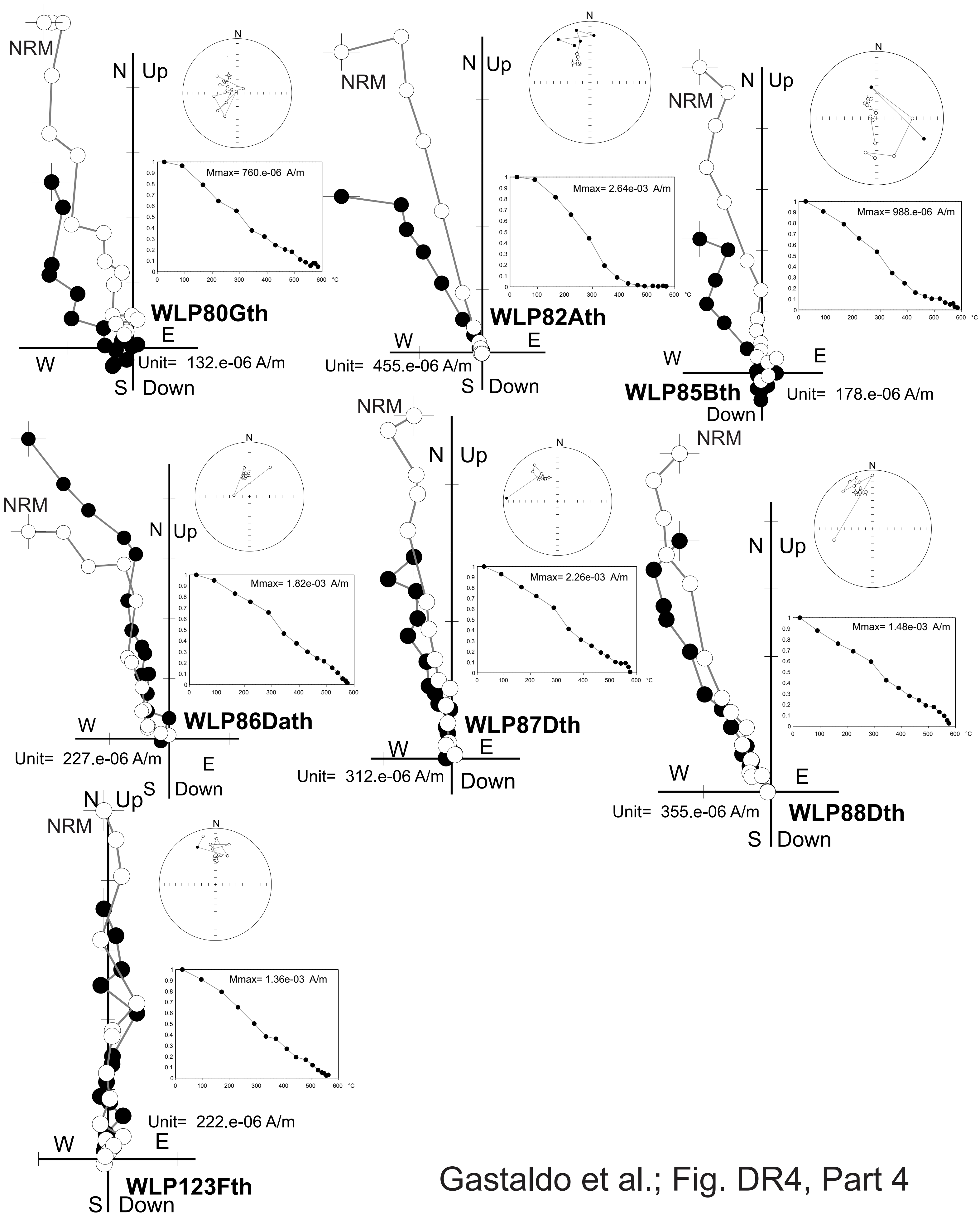

Gastaldo et al.; Fig. DR4, Part 4

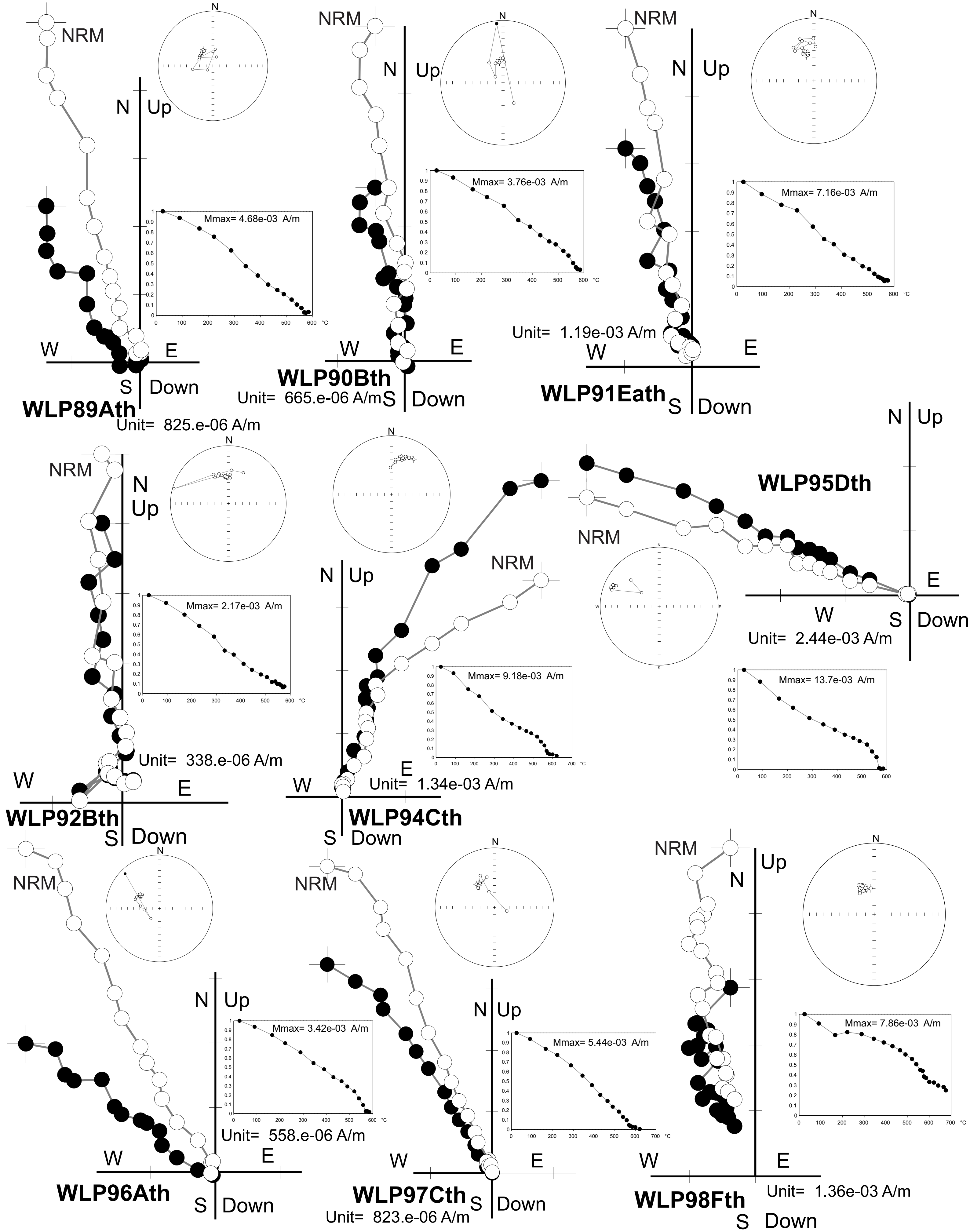

Gastaldo et al.; Fig. DR4, Part 5

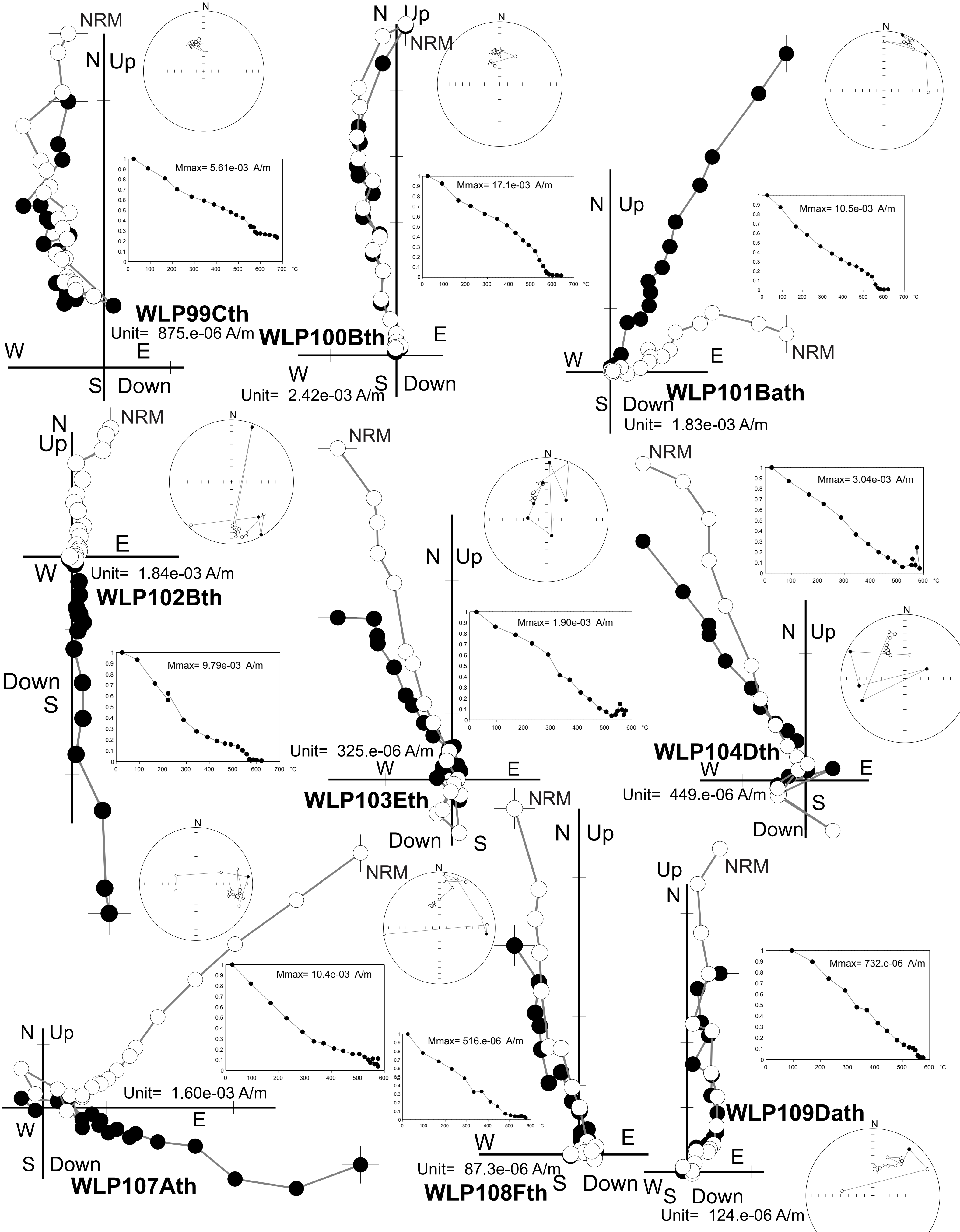

Gastaldo et al.; Fig. DR4, Part 6

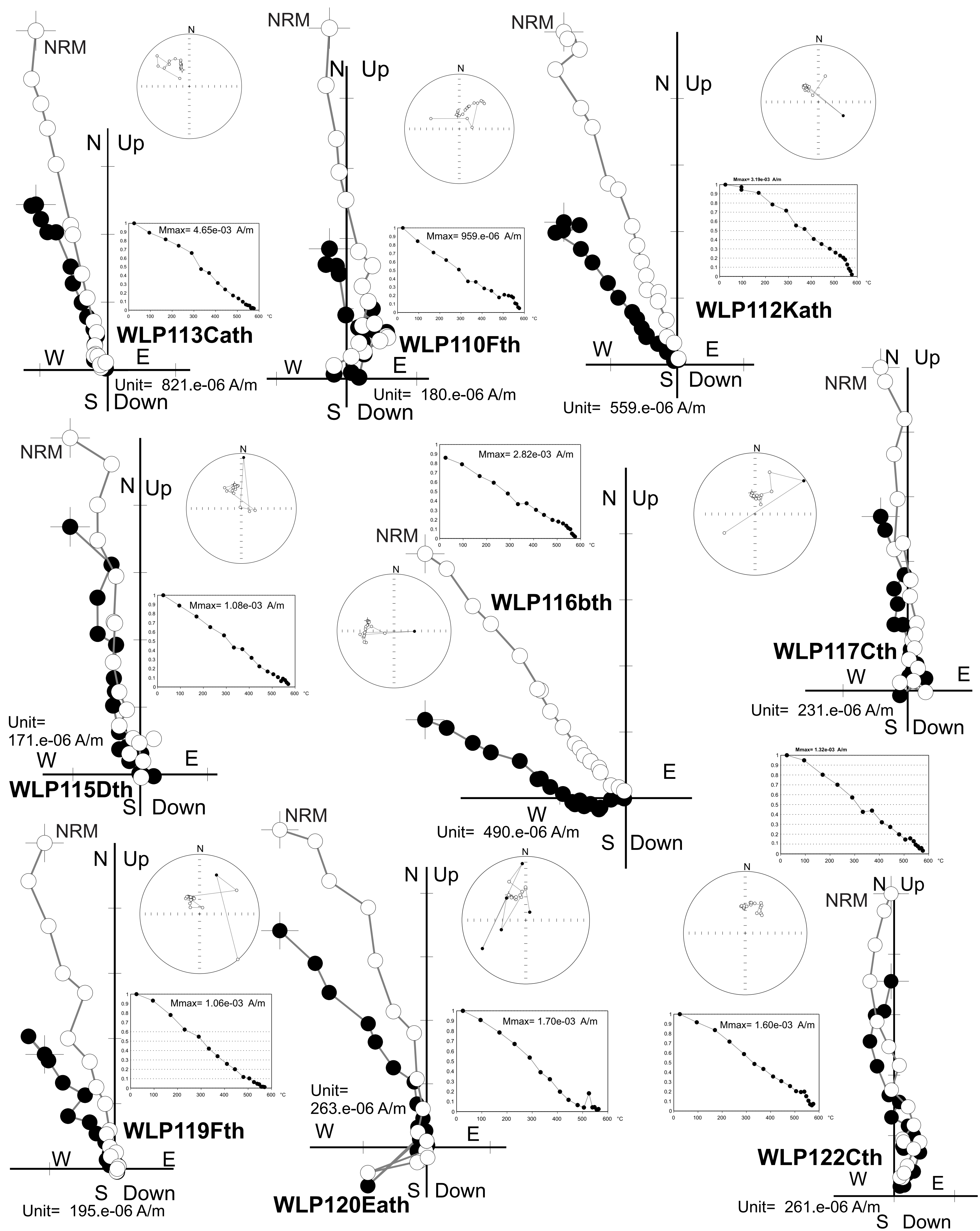

Gastaldo et al.; Fig. DR4, Part 7

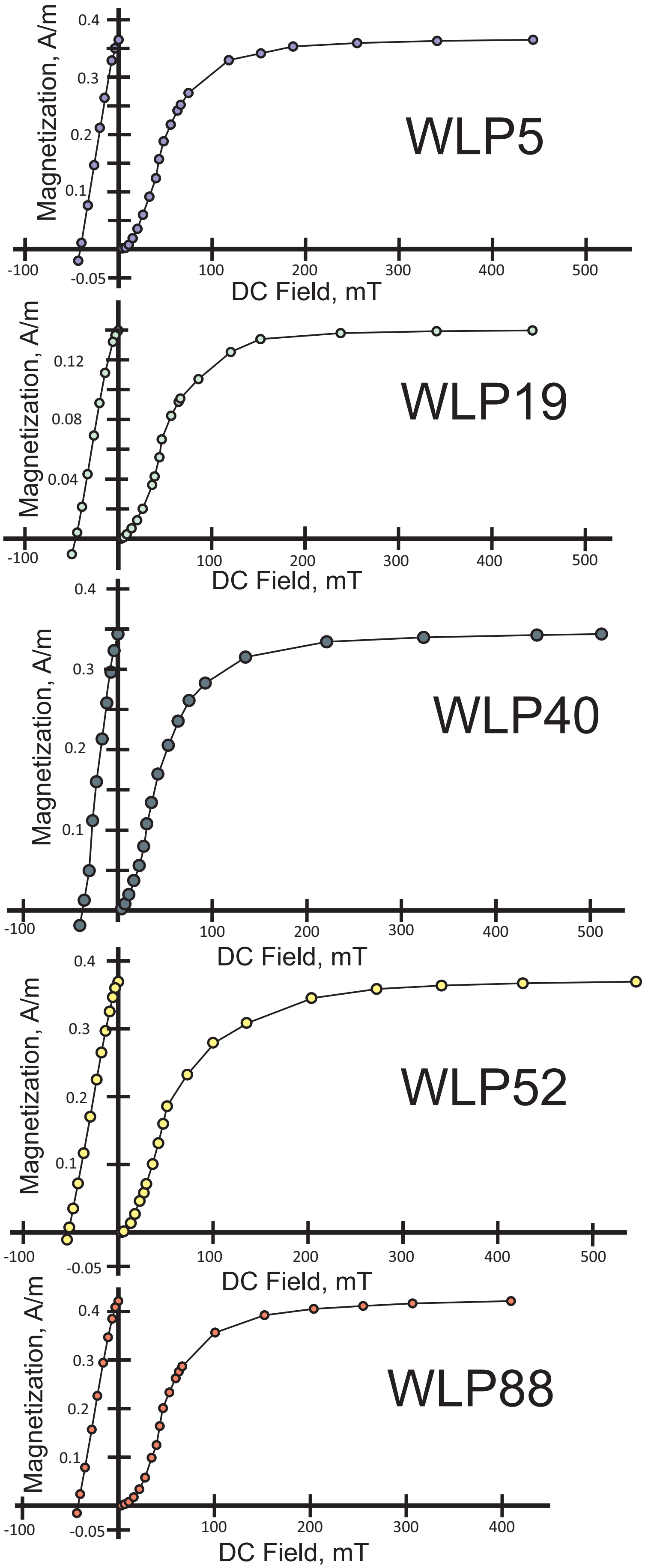

Gastaldo et al.; Fig. DR5

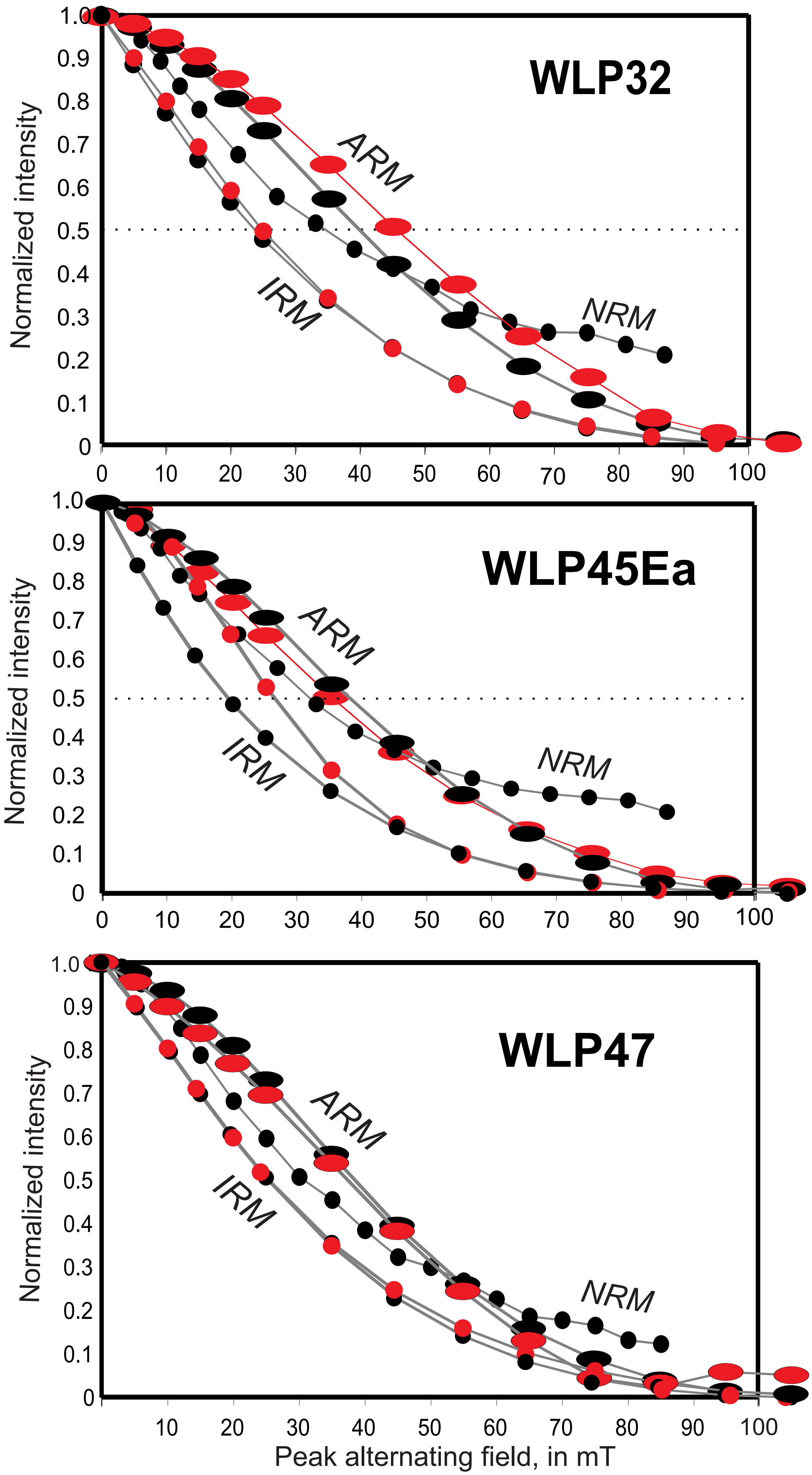

Gastaldo et al.; Fig. DR6, Part 1

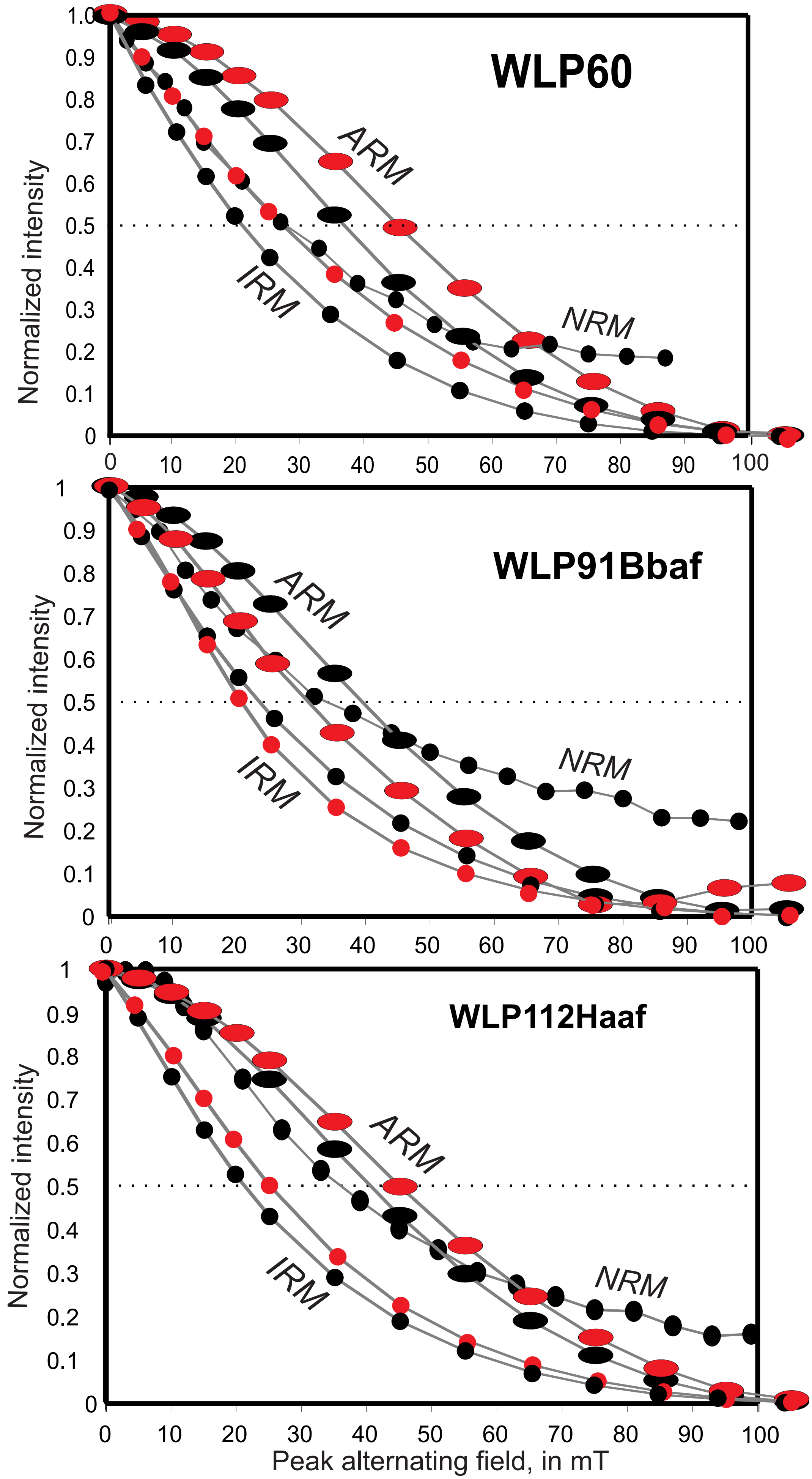

Gastaldo et al.; Fig. DR6, Part 2

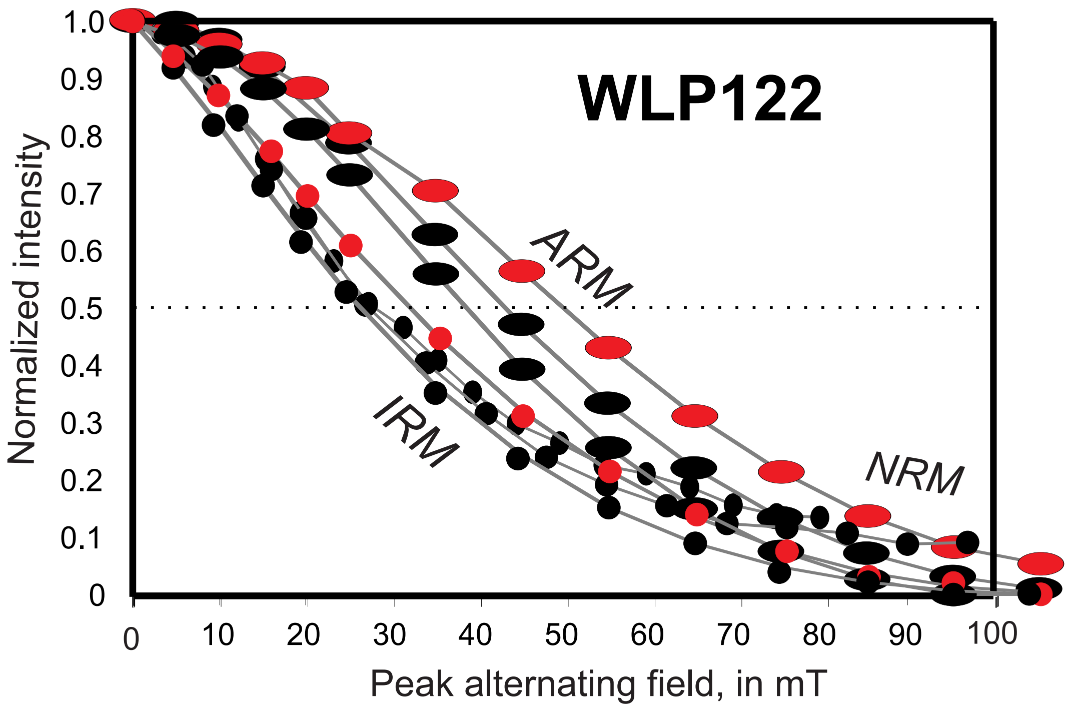

Gastaldo et al.; Fig. DR6, Part 3

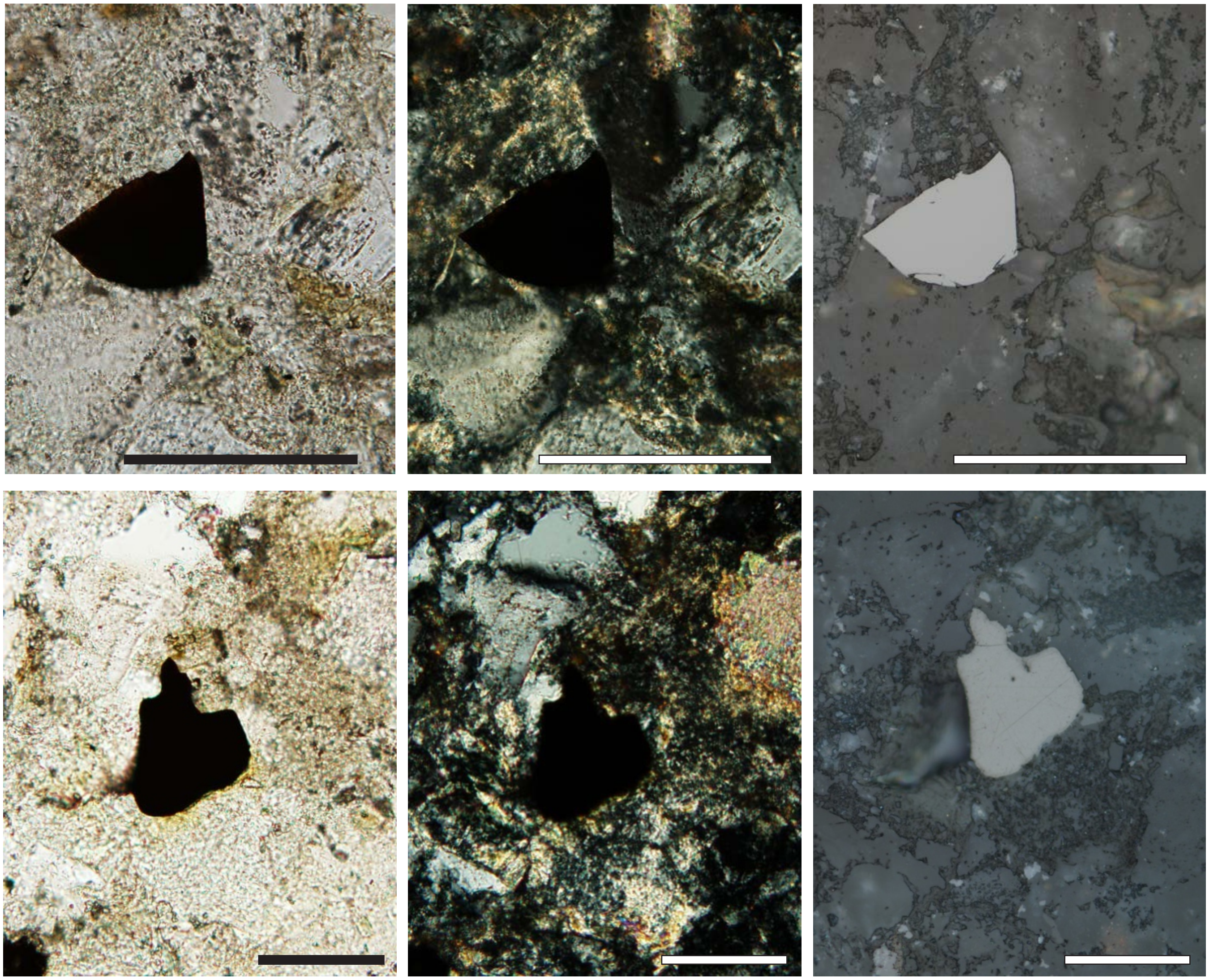

Transmitted Light

Transmitted Light
Crossed Polars

Reflected Light
Uncrossed Polars

Gastaldo et al.; Fig. DR7

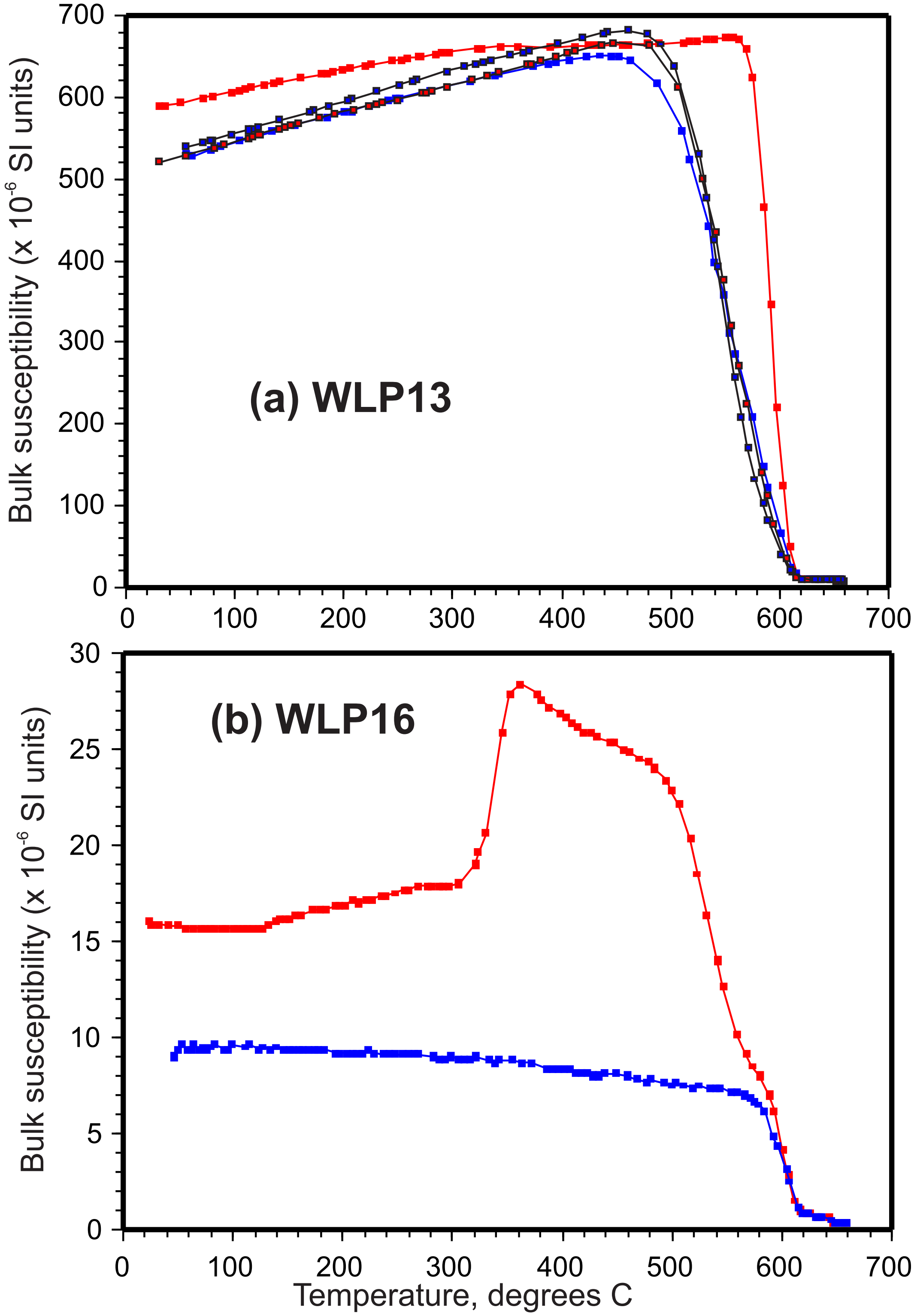

Gastaldo et al.; Fig. DR8

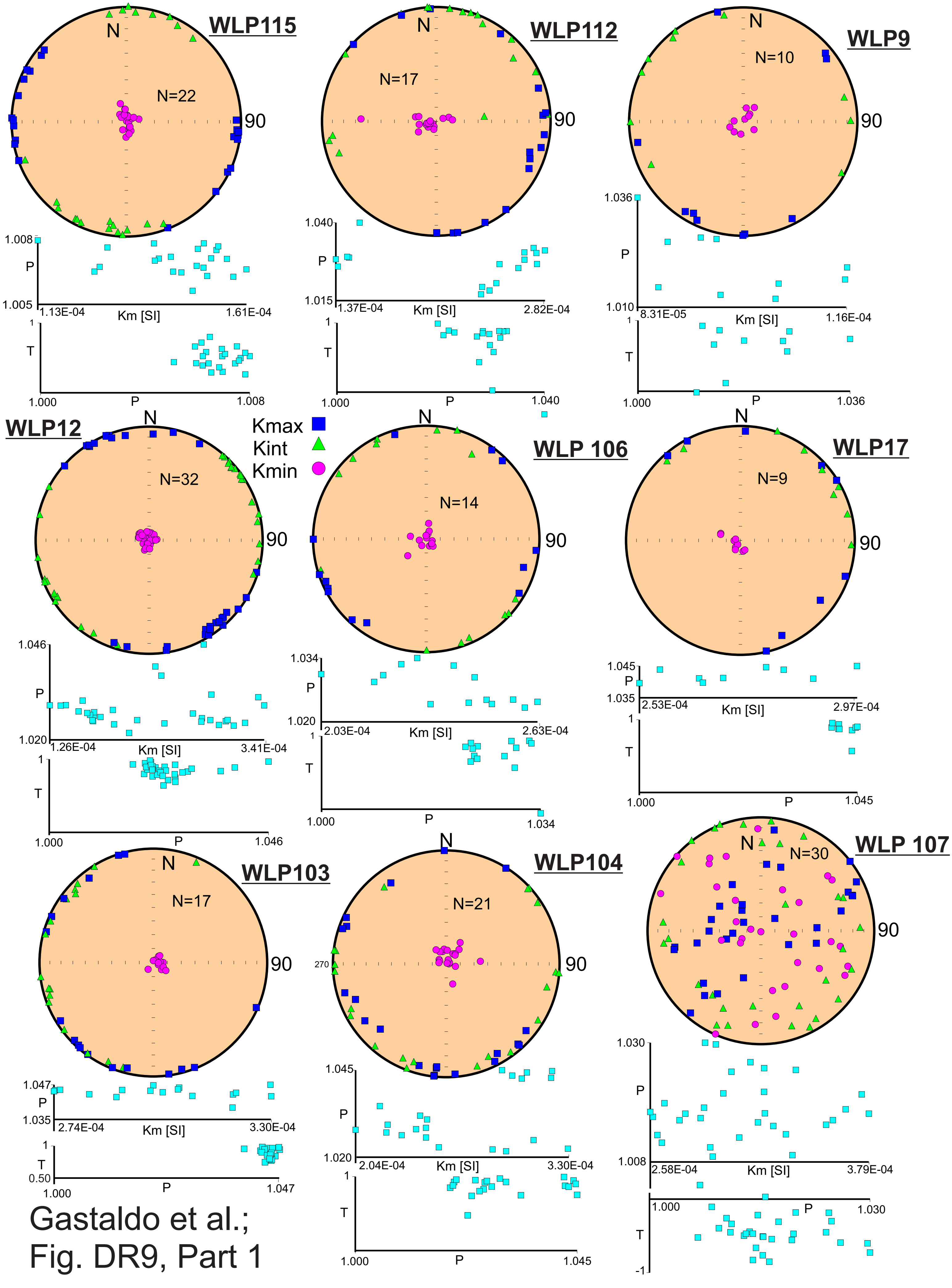

Gastaldo et al.;
Fig. DR9, Part 1

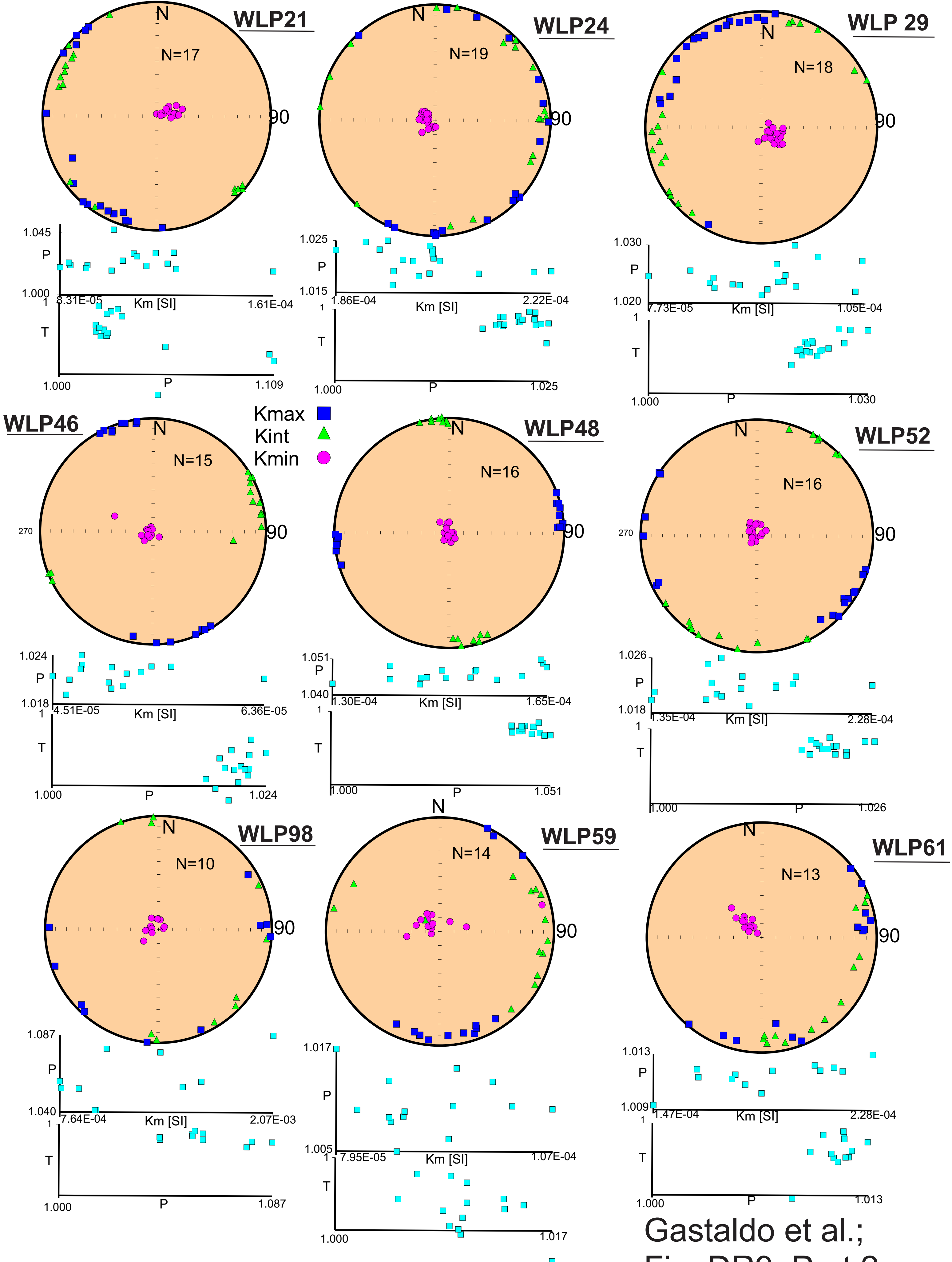

Gastaldo et al.;
Fig. DR9, Part 2

Table DR1

U-Pb isotopic data for single chemically abraded zircon grains from a porcellanite layer at Old Lootsberg Pass, Karoo Basin, South Africa.

No.	PbC (pg)	Pb*/ Pbc (c)	Th/U	206Pb/ 204Pb measured	207Pb/ 235U	2 σ	206Pb/ 238U	2 σ	corr coef	207Pb/ 206Pb	2 Sig	207Pb/ 235U Age (Ma)	2 σ	206Pb/ 238U Age (Ma)	2 σ
1	0.3	14.6	1.0	816	0.4609	0.0093	0.04780	0.00014	0.653	0.0699	0.0013	385	6	300.97	0.89
2	0.6	4.9	1.2	274	0.2841	0.0142	0.04047	0.00015	0.848	0.0509	0.0024	254	11	255.77	0.91
3	0.2	27.5	0.7	1636	0.2853	0.0037	0.04027	0.00013	0.462	0.0514	0.0006	255	3	254.54	0.79
4	0.2	39.3	1.5	1956	0.2849	0.0031	0.04027	0.00005	0.628	0.0513	0.0005	255	2	254.52	0.33
5	0.2	31.6	1.0	1749	0.2854	0.0070	0.04016	0.00010	0.646	0.0515	0.0012	255	5	253.83	0.64
6	0.2	36.2	1.0	1981	0.2820	0.0027	0.04013	0.00010	0.454	0.0510	0.0005	252	2	253.66	0.60
7	0.2	46.5	0.7	2733	0.2798	0.0019	0.04011	0.00006	0.517	0.0506	0.0003	251	1	253.54	0.38
8	0.2	63.2	1.0	3435	0.2836	0.0016	0.04011	0.00005	0.526	0.0513	0.0003	254	1	253.53	0.32
9	0.2	19.0	1.8	893	0.2908	0.0048	0.04010	0.00008	0.620	0.0526	0.0008	259	4	253.47	0.50
10	0.2	45.4	1.0	2505	0.2835	0.0019	0.04009	0.00005	0.540	0.0513	0.0003	253	2	253.40	0.30
11	0.7	19.8	1.5	977	0.2855	0.0040	0.04008	0.00006	0.668	0.0517	0.0007	255	3	253.33	0.34

All grains pretreated by thermal annealing and Hf etch (chemical abrasion; Mattinson, 2005).

PbC is total common Pb in analysis.

Pb*/Pbc is ratio of radiogenic Pb to common Pb.

206Pb/204Pb measured ratio corrected for common Pb in spike and fractionation only.

Th/U calculated from radiogenic ^{208}Pb/^{206}Pb ratio and ^{207}Pb/^{206}Pb age assuming concordance.

Pb/U ratios corrected for fractionation, common Pb in spike and blank . All common Pb assumed to be blank (blank isotopic composition: ^{206}Pb/^{204}Pb: 18.22, ^{207}Pb/^{204}Pb: 15.61, ^{208}Pb/^{204}Pb: 39.36 (2σ erro

Corrected for initial Th/U disequilibrium using radiogenic 208Pb and Th/U[magma] = 4.2.

Corr. coef. = correlation coefficient.

Ages calculated using the decay constants λ238 = 1.55125E-10 and λ235 = 9.8485E-10 (Jaffey et al. 1971).

Table DR2. Drilled samples for magnetostratigraphy, stratigraphic height at which samples originate, lithology, GPS site coordinates (WGS 80) and elevation, and waypoint date/time

Sample	Strat Height	Lithology	Latitude	Longitude	Aggregate Elevation	Waypoint Date/Time
P01	6.8	fwacke	-31.804933	24.806586	1559.468262	5/10/2013 12:34
P02	11.8	fwacke	-31.804188	24.806044	1565.490356	5/10/2013 12:47
P03	13.4	cs	-31.80404	24.805839	1566.633545	5/10/2013 12:55
P05	15.3	cs	-31.803688	24.80557	1568.775146	5/10/2013 12:59
P04	14.7	fwacke	-31.803549	24.805749	1568.427002	5/10/2013 13:11
P06	15.3	cs	-31.803537	24.805691	1569.000244	5/10/2013 13:14
P07	17.8	vfwacke	-31.803304	24.805666	1570.360352	5/10/2013 13:17
P08	19	vfwacke	-31.803215	24.805686	1570.752441	5/10/2013 13:22
P09	19.15	vfwacke	-31.803149	24.805648	1571.025269	5/10/2013 13:25
P10	20.4	vfwacke	-31.802886	24.805473	1571.578369	5/10/2013 13:29
P11	20.2	cs	-31.802862	24.805365	1571.664429	5/10/2013 13:32
P12	20.3	cs	-31.802788	24.805316	1571.810791	5/10/2013 13:35
P13	24.4	cs	-31.802633	24.804806	1574.88916	5/10/2013 13:39
P14	24.65	vfwacke	-31.802526	24.804673	1574.706665	5/10/2013 13:42
P15	24.7	vfwacke	-31.802415	24.804698	1576.21521	5/10/2013 13:45
P16	27.15	vfwacke	-31.802404	24.804501	1579.294678	5/10/2013 13:48
P17	27.6	cs	-31.802066	24.80426	1579.066406	5/10/2013 13:51
P18	28.8	cs	-31.801902	24.804112	1578.163208	5/10/2013 13:54
P19	29	cs	-31.801808	24.804141	1579.843994	5/10/2013 13:57
P20	29	cs	-31.801777	24.80411	1579.305786	5/10/2013 13:58
P21	29.8	vfwacke	-31.801748	24.804113	1580.240479	5/10/2013 14:00
P22	33	vfwacke	-31.801425	24.804088	1582.699219	5/10/2013 14:03
P23	37.65	vfwacke	-31.801156	24.804171	1586.765259	5/10/2013 14:06
P24	38.65	vfwacke	-31.800984	24.804192	1587.784302	5/10/2013 14:08
P25	40	vfwacke	-31.800764	24.804368	1589.258545	5/10/2013 14:11
P26	40.8	cs	-31.800515	24.804304	1590.240723	5/10/2013 14:17
P27	41.95	cs	-31.800317	24.804328	1590.54248	5/10/2013 14:20
P28	43.25	vfwacke	-31.80028	24.804263	1592.216675	5/10/2013 14:22
P29	52	vfwacke	-31.79899	24.802446	1602.64978	5/10/2013 14:29
P30	54.6	vfwacke	-31.798866	24.802315	1605.581909	5/10/2013 14:32
P31	59	concretion	-31.79909	24.80142	1609.997803	5/10/2013 14:36
P32	60.5	vfwacke	-31.798995	24.801236	1611.970703	5/10/2013 14:39
P33	61.7	vfwacke	-31.79904	24.801242	1611.982544	5/10/2013 14:42
P34	61.9	cs	-31.798921	24.801118	1611.791016	5/10/2013 14:44
P35	67.05	vfwacke	-31.798348	24.800508	1617.373779	5/10/2013 14:50
P36	68.05	sandy cs	-31.798215	24.800438	1619.107544	5/10/2013 14:52
P37	68.5	vfwacke	-31.79825	24.800301	1619.236572	5/10/2013 14:57
P38	76.15	cs	-31.797488	24.799705	1626.646973	5/10/2013 15:05
P39	77.95	vfwacke	-31.797138	24.799481	1641.314087	5/11/2013 12:03
P40	80.1	vfwacke	-31.797108	24.799338	1641.394043	5/11/2013 12:05
P41	80.6	vfwacke	-31.797018	24.799316	1642.054932	5/11/2013 12:07
P42	82.95	vfwacke	-31.796863	24.799359	1643.662231	5/11/2013 12:10
P43	86.8	vfwacke	-31.796723	24.799021	1646.390259	5/11/2013 12:13
P44	89.1	vfwacke	-31.79656	24.799076	1646.967529	5/11/2013 12:16
P45	90.7	concretion	-31.796366	24.799075	1648.056641	5/11/2013 12:19
P46	92.45	vfwacke	-31.796242	24.799126	1649.034912	5/11/2013 12:21
P48	96.85	vfwacke	-31.795662	24.799003	1654.99353	5/11/2013 12:27
P49	98.75	cs	-31.795393	24.79886	1656.514038	5/11/2013 12:30
P50	101.6	vfwacke	-31.795125	24.798815	1659.856079	5/11/2013 12:34
P51	102.85	vfwacke	-31.795047	24.798754	1660.164795	5/11/2013 12:36
P52	106.35	vfwacke	-31.794963	24.798773	1663.40686	5/11/2013 12:41
P53	++	vfwacke	-31.793308	24.800317	1685.843262	5/12/2013 7:44
P54	++	concretion	-31.79355	24.801691	1693.051636	5/12/2013 7:48

P55	++	vfwacke	-31.793492	24.80269	1699.123657	5/12/2013 7:52
P56	++	vfwacke	-31.794202	24.803447	1703.671875	5/12/2013 7:55
P57	++	concretion	-31.794052	24.804356	1708.597656	5/12/2013 8:01
P58	++	concretion	-31.794052	24.804356	1708.597656	5/12/2013 8:01
P59	++	cs	-31.79357	24.805172	1714.472168	5/12/2013 8:04
P60	++	vfwacke	-31.79366	24.80531	1716.139404	5/12/2013 8:06
P60 22JAN14	++	resampled….PNC	-31.794494	24.80619		1/22/2014 7:15
P61	++	vfwacke	-31.794542	24.806152	1723.556274	5/12/2013 8:10
P62	++	vfwacke	-31.794708	24.807562	1733.682617	5/12/2013 8:15
P63	++	vfwacke	-31.79462	24.806318	1722.728882	5/12/2013 8:25
P80	105.8	vfwacke	-31.795478	24.796655	1666.201538	1/18/2014 11:23
P81	111.8	vfwacke	-31.795295	24.796581	1667.749023	1/18/2014 11:26
P82	113.8	nodules	-31.794883	24.79642	1670.015747	1/18/2014 11:31
P83	113.8	cs	-31.79485	24.796422	1669.423828	1/18/2014 11:32
P84	116	vfwacke	-31.794719	24.796341	1672.471313	1/18/2014 11:33
P85	116.5	vfwacke	-31.794645	24.796318	1674.701294	1/18/2014 11:40
P86	118	cs	-31.794547	24.796332	1675.937988	1/18/2014 11:41
P87	119.5	sandy cs	-31.79443	24.796301	1677.272217	1/18/2014 11:43
P88	120	vfwacke	-31.794359	24.79633	1679.493896	1/18/2014 11:45
P89	120	vfwacke	-31.794256	24.796184	1680.358032	1/18/2014 11:47
P90	123.5	cs	-31.793938	24.795962	1685.46167	1/18/2014 11:50
P91	124	cs	-31.79381	24.795891	1688.223633	1/18/2014 11:51
P92	130.5	siltstone	-31.793767	24.795881	1689.983643	1/18/2014 11:54
P93	130.5	nodules	-31.793671	24.795863	1694.018311	1/18/2014 11:56
P94	132	sandy cs	-31.793607	24.795861	1695.946167	1/18/2014 11:59
P95	134	vfwacke	-31.793581	24.795867	1696.931641	1/18/2014 12:01
P96	134.5	vfwacke	-31.79354	24.795792	1697.687256	1/18/2014 12:02
P97	136	cs	-31.793503	24.795756	1699.306885	1/18/2014 12:06
P98	137.6	cs	-31.79339	24.795599	1703.302368	1/18/2014 12:08
P99	138	cs	-31.793329	24.79545	1707.144409	1/18/2014 12:10
P100	138.2	cs	-31.793267	24.795364	1709.672607	1/18/2014 12:18
P101	137.5	cs	-31.793297	24.795379	1711.358765	1/18/2014 12:14
P102	142.2	PNC	-31.793237	24.795304	1713.261597	1/18/2014 12:22
P103		cs	0.05 m above P17			
P104		cs	0.10 m above P17			
P105	`	cs	0.6 m above P17, 0.25 m below P18			
P106		cs	eqiv to P 16			
P107		concretions	~ 1.1 m above P17			
P108		cs	0.10 above P13			
P109		vfwacke	0.5 m below P15			
P110		vfwacke	0.25 m below P15			
P111		vfwacke	0.1 m below P110			
Sample sites below the base of the stratigraphic column illustrated in current manuscript						
P112	-9	vfwacke	-31.808272	24.80511	1537.83606	1/21/2014 9:06
P113	-10.2	vfwacke	-31.808539	24.80483	1537.308716	1/21/2014 8:08
P114	-10.6	nodules	-31.808454	24.804901	1537.223145	1/21/2014 8:11
P115	-13.3	vfwacke	-31.809509	24.804618	1533.482544	1/21/2014 7:43
P116	-15.8	vfwacke	-31.811576	24.803864	1528.624878	1/21/2014 7:03
P117	-16.4	sandy cs	-31.811635	24.803944	1526.652832	1/21/2014 6:58
P118	-16.9	sandy cs	-31.81167	24.803779	1526.321655	1/21/2014 6:50
P119	-18.3	sandy cs	-31.811877	24.803831	1522.781128	1/21/2014 6:41
P120	-19.6	cs	-31.811884	24.803928	1519.530151	1/21/2014 6:33
P121	-6.4	sandy cs	-31.80746	24.8052	1545.25	1/21/2014 9:38
P122	-4.6	sandy cs	-31.80693	24.806159	1549.737061	1/21/2014 11:00
P123	-2.9	cs	-31.806154	24.806585	1550.76355	1/21/2014 11:28
KEY						

++	Site in correlative section; see Figure 1
PNC	Pedogenic Nodule Conglomerate
vfwacke	Very Fine Wacke
sandy cs	Sandy Coarse Siltstone
cs	Coarse siltstone
slitstone	siltstone
concretions	concretions